Molecular Biology of the Cell
Vol. 15, 4971–4989, November 2004

Stable and Dynamic Axes of Polarity Use Distinct Formin Isoforms in Budding Yeast[D] [V]

David Pruyne,* Lina Gao,* Erfei Bi,† and Anthony Bretscher*‡

*Department of Molecular Biology and Genetics, Cornell University, Ithaca, NY 14853-2703; and †Department of Cell and Developmental Biology, University of Pennsylvania School of Medicine, Philadelphia, PA 19104-6018

Submitted April 8, 2004; Revised September 1, 2004; Accepted September 2, 2004
Monitoring Editor: Tim Stearns

Bud growth in yeast is guided by myosin-driven delivery of secretory vesicles from the mother cell to the bud. We find transport occurs along two sets of actin cables assembled by two formin isoforms. The Bnr1p formin assembles cables that radiate from the bud neck into the mother, providing a stable mother-bud axis. These cables also depend on septins at the neck and are required for efficient transport from the mother to the bud. The Bni1p formin assembles cables that line the bud cortex and target vesicles to varying locations in the bud. Loss of these cables results in morphological defects as vesicles accumulate at the neck. Assembly of these cables depends on continued polarized secretion, suggesting vesicular transport provides a positive feedback signal for Bni1p activation, possibly by rho-proteins. By coupling different formin isoforms to unique cortical landmarks, yeast uses common cytoskeletal elements to maintain stable and dynamic axes in the same cell.

INTRODUCTION

Proper cell polarization requires a balance between dynamism and stability. Persistent systems, such as the apical and basolateral domains of epithelial cells, show a higher stability than flexible systems, such as cells undergoing chemotaxis. However, both types can use similar cytoskeletal components, so an important task in understanding the control of polarity is to identify features that influence persistence, and how those features integrate with the core cytoskeletal machinery providing the physical expression of polarity.

The process of bud growth of the yeast *Saccharomyces cerevisiae* provides a model for examining the control of polarity (for reviews, see Bretscher, 2003; Chang and Peter, 2003). Secretory organelles, such as the Golgi and endoplasmic reticulum, are distributed throughout the bud and mother cell, whereas post-Golgi secretory vesicles concentrate at discrete growth sites at the cell cortex. These vesicles are guided to these sites along what are essentially two axes of polarity: a stable axis directing traffic from the mother into the bud, and a dynamic axis that fine-tunes delivery from the bud neck to specific regions in the bud, sending vesicles first to the small bud tip, then to the entire bud surface, and finally back toward the neck during mother/daughter separation. On delivery to these locations, post-Golgi vesicles fuse with the cell surface to promote localized cell expansion.

Article published online ahead of print. Mol. Biol. Cell 10.1091/mbc.E04–04–0296. Article and publication date are available at www.molbiolcell.org/cgi/doi/10.1091/mbc.E04–04–0296.

[D] [V] The online version of this article contains supplementary material accessible through http://www.molbiolcell.org.

‡ Corresponding author. E-mail address: apb5@cornell.edu.

Abbreviations used: FH, formin homology.

Two class-V myosins, with heavy chains encoded by *MYO2* (Johnston *et al*., 1991) and *MYO4* (Haarer *et al*., 1994), propel cellular components, including vesicles, organelles, mRNAs, and microtubules, from the mother into the bud during growth and organelle segregation. The myosins move along cables of actin filaments that radiate throughout the cell in arrays oriented toward growth sites (Adams and Pringle, 1984; Kilmartin and Adams, 1984).

Assembly of these cables depends on two formin homologues, Bni1p and Bnr1p (Evangelista *et al*., 2002; Sagot *et al*., 2002a), members of a family of cytoskeletal regulatory proteins defined by conserved formin homology (FH)1 and FH2 domains (for reviews, see Evangelista *et al*., 2003; Wallar and Alberts, 2003). In vitro, the FH2 domain nucleates actin filaments from monomers (Pruyne *et al*., 2002; Sagot *et al*., 2002b; Kovar *et al*., 2003; Li and Higgs, 2003; Harris *et al*., 2004; Kobielak *et al*., 2004), but distinct from other nucleators, it remains associated with the growing barbed end to promote elongation, even in the presence of barbed-end capping proteins (Pruyne *et al*., 2002; Kovar *et al*., 2003; Li and Higgs, 2003; Pring *et al*., 2003; Harris *et al*., 2004; Kobielak *et al*., 2004; Moseley *et al*., 2004). The FH1 region is a proline-rich stretch that recruits profilin, an actin-monomer binding protein essential for formin function in vivo (Evangelista *et al*., 2002), to participate in FH2-mediated nucleation in vitro (Sagot *et al*., 2002b; Kovar *et al*., 2003; Pring *et al*., 2003). Other regions present in Bni1p and Bnr1p are a regulatory NH_2-terminal rho-GTPase-binding domain that subjects many formins to rho-dependent activation (Kohno *et al*., 1996; Evangelista *et al*., 1997; Imamura *et al*., 1997; Dong *et al*., 2003), and an FH3 motif that helps localize formins within the cell (Petersen *et al*., 1998).

With loss of formin function, actin cables disassemble in 2 min, and a cytokinetic ring is unable to assemble, but actin patches remain intact (Evangelista *et al*., 2002; Sagot *et al*., 2002a; Tolliday *et al*., 2002). Other actin nucleators, particularly the Arp2/3 complex, play no apparent role in cable or

cytokinetic ring assembly in budding yeast (Winter *et al*., 1999; Evangelista *et al*., 2002; Tolliday *et al*., 2002), suggesting the formins might be in vivo nucleators for these actin filaments. However, the loss of Bni1p or Bnr1p individually results in different phenotypes. To determine whether these distinct phenotypes relate to actin assembly, we examined the relationship between the two formins and patterns of filament assembly in the yeast cell.

MATERIALS AND METHODS

Plasmid Construction

To allow for overexpression of *CLN2*, a 694-base pair *Bam*HI/*Eco*RI fragment from pRS316-GAL1 (Liu *et al*., 1992) containing the promoter of the *GAL1* and *GAL10* genes, was cloned into pRS306 (Sikorski and Hieter, 1989) to generate pDP132. The *CLN2* ORF with 201 base pairs downstream sequence and introduced flanking *Bam*HI and *Not*I sites was amplified by polymerase chain reaction (PCR) from genomic DNA by using primers GGCGGATCCATGGCTAGTGCTGAACCAAGACCCC and GGGCGGCCGCTCTACACAGAATTTAGTTGGCTGT (restriction sites underlined), cloned into pCR2.1 by the TOPO-TA Cloning reaction (Invitrogen, Carlsbad, CA), and sequenced to verify the absence of mutations. The *Bam*HI/*Not*I fragment of this was then cloned into pDP132 to generate pDP134.

To allow for visualization of Bud6p, a 4.0-kb *Eco*RI/*Sal*I fragment from pRB2190 (Amberg *et al*., 1997), containing a functional NH_2-terminal green fluorescent protein (GFP)^{S65T} fusion of the *BUD6* open reading frame (ORF) flanked by the *ACT1* promoter and terminator, was subcloned into pRS306 to generate pDP128. For visualization of Cdc12p, a 2.8-kb *Eco*RI/*Sst*I fragment from pRS315::*GFP:CDC12* (Richman *et al*., 1999), containing an NH_2-terminal GFP-fusion of *CDC12* behind the *CDC12* promoter, was cloned into pRS306 to generate pDP135. For visualization of Bni1p in vivo, the *BNI1* ORF plus promoter from plasmid p39C2 (*CEN LEU2*; kindly provided by H. Fares and J.R. Pringle, University of North Carolina, Chapel Hill, NC) was COOH-terminally tagged in-frame with *GFP*$^{F64L/S65T}$ by a PCR-based method (Longtine *et al*., 1998). A 11.6-kb *Sph*I/*Spe*I fragment from this plasmid, carrying *BNI1* promoter, *BNI1:GFP* ORF, and *Kan*^{R}, was subcloned into YEplac181 (2 μm *LEU2*; Gietz and Sugino, 1988) to generate YEp181-*BNI1:GFP::Kan*^{R}.

To allow for deletion of *TPM2* by using a *TRP1* marker, three individual PCRs were done to amplify the *TRP1* sequence by using primers CGCGGCGGGTGTGGTGGTTA and AGCGGGTGTTGGCGGGTGTA, bases –716 to –209 upstream of *TPM2* by using primers GACCAATGGGCACGGAAGG (with endogenous *Kpn*I site) and GTAACCACCACACCCGCCGCGTGTTGAAATACTTGTAAAAA, and bases +488 to +780 downstream of *TPM2* by using primers AAAGCTGACGCAACGATTACTAT (with endogenous *Nde*I site) and GACACCCGCCAACACCCGCTCCCATTGATAAGACTAAAA (*TRP1*-complementing sequences underlined). Resultant products were combined by double fusion PCR (Amberg *et al*., 1995) to generate *TRP1* flanked by *TPM2* upstream and downstream sequences, and then was cloned into pCR2.1 by the TOPO-TA Cloning method (Invitrogen) to generate pDP116.

For overproduction of NH_2-terminally truncated Bnr1p in yeast, plasmid p015 containing Bnr1p residues 386-1375 behind the *GAL1-10* promoter was isolated as a suppressor of the temperature-sensitive growth of ABY2000 (*bni1-11 bnr1*Δ) by using a *GAL1*-regulated cDNA expression library (Liu *et al*., 1992). For production of recombinant Bnr1p sequences including the FH1, FH2, and COOH-terminal residues fused to glutathione *S*-transferase (GST) [called GSTBnr1p(FH1FH2)], *BNR1* sequence from +2269 to +4284 was amplified from genomic DNA by using primers CCGGAATTCCCCAAGTAGTACCTGAAGTTGTTAAACTACC and GCAGCATGGCGGCCGCGAATCTGTCCATCTCCAAATC (*Eco*RI and *Not*I restriction sites, respectively, underlined) and cloned into the *Eco*RI/*Not*I sites of pGEX-6P-3 (Amersham Biosciences, Piscataway, NJ) to generate p080. The *BNR1* sequence was analyzed to verify the absence of mutations.

Yeast Strains and Growth Conditions

The genotypes of yeast strains used are listed in Table 1. Growth conditions and temperature shifts were done as described previously (Pruyne *et al*., 1998; Evangelista *et al*., 2002).

Strains ABY1637 (*tpm2*Δ *cdc10-1*), ABY1638 (*tpm2*Δ *cdc10-1*), ABY1639 (*tpm1-2 tpm2*Δ *cdc10-1*), ABY1641 (*tpm2*Δ *cdc12-6*), ABY1643 (*tpm1-2 tpm2*Δ *cdc12-6*) were generated through crosses between M-195 (*cdc10-1*) or M-239 (*cdc12-6*) (both kindly provided by M. Longtine, Oklahoma State University, Stillwater, OK) and ABY944 (*tpm1-2 tpm2*Δ) or ABY945 (*tpm2*Δ), followed by backcross of the appropriate isolates to ABY944 or ABY945 and sporulation. ABY1662 (*cdc10-1/cdc10-1 tpm2*Δ*/tpm2*Δ) was generated from ABY1637 mated to ABY1638.

For comparison of *bni1* and septin mutant phenotypes, ABY1637 was crossed with Y4133 (*bni1-11 bnr1*Δ) and sporulated to generate ABY2201 (*cdc10-1 tpm2*Δ), ABY2209 (*bni1-11*), ABY2218 (*bni1-11 bnr1*Δ), and ABY2226 (*bni1-11 cdc10-1*), or progeny were mated appropriately to generate ABY2247 (*bni1-11/bni1-11 tpm2*Δ*/tpm2*Δ) and ABY2248 (*bni1-11/bni1-11 cdc10-1/cdc10-1 tpm2*Δ*/tpm2*Δ). The retention of *tpm2*Δ in many of the *BNR1*+ strains reflects genetic linkage between the *TPM2* and *BNR1* loci. However, in the presence of wild-type *TPM1*, we find no effects from *tpm2*Δ and believe this deletion has not influenced results obtained.

To generate yeast with inducible *CLN2*, *Spe*I-linearized pDP134 was transformed into Y1239 (wild-type) and ABY1807 (*tpm1-2 tpm2*Δ), resulting in integration at the *CLN2* locus to yield ABY2251 (*GAL-CLN2*) and ABY2252 (*tpm1-2 tpm2*Δ *GAL-CLN2*). To generate yeast bearing a control plasmid or an inducible NH_2-terminally truncated Bni1p or Bnr1p, Y1239 was transformed with pRS316 (Sikorski and Hieter, 1989), p356 (Bni1p residues 452-1953) (Evangelista *et al*., 2002), or p015, respectively.

For visualization of Sec4p in vivo, ABY1848 (wild type), ABY1867 (*bni1*Δ*/bni1*Δ), and ABY1801 (*bnr1*Δ*/bnr1*Δ) were transformed with pRC651, a construct identical to reported pRC556 (pRS315::*GFP:SEC4*; Schott *et al*., 2002). For visualization of Bni1p in vivo, ABY1848 was transformed with YEp181-*BNI1:GFP::Kan*^{R}.

For visualization of Bud6p, pDP128 was *Stu*I-linearized and transformed into ABY987 (*tpm2*Δ*/tpm2*Δ) and ABY988 (*tpm1-2/tpm1-2 tpm2*Δ*/tpm2*Δ) for integration at the *ura3-52* locus. Sporulation and mating of Ura+ haploids yielded ABY1199 (*tpm2*Δ*/tpm2*Δ *GFP:BUD6/GFP:BUD6*) and ABY1171 (*tpm1-2/tpm1-2 tpm2*Δ*/tpm2*Δ *GFP:BUD6/GFP:BUD6*).

For visualization of Spa2p, pRS406S2G bearing a COOH-terminal *GFP*^{S65T}-fusion of *SPA2* (Arkowitz and Lowe, 1997) was *Stu*I linearized and integrated at the *ura3-52* locus in ABY971 (*tpm1-2/tpm1-2 tpm2*Δ*/tpm2*Δ) and ABY973 (*tpm2*Δ*/tpm2*Δ) to generate ABY1197 (*tpm1-2/tpm1-2 tpm2*Δ*/tpm2*Δ *SPA2:GFP/SPA2:GFP*) and ABY1198 (*tpm2*Δ*/tpm2*Δ *SPA2:GFP/SPA2:GFP*).

For visualization of Cdc12p, pDP135 was *Mlu*I linearized and integrated at one *CDC12* locus of ABY1848 to generate ABY1896 (*CDC12/CDC12::URA3::GFP:CDC12*), into ABY1662 to generate ABY2257 (*CDC12/CDC12::URA3::GFP:CDC12 cdc10-1/cdc10-1 tpm2*Δ*/tpm2*Δ), into ABY1867 to generate ABY1898 (*bni1*Δ*/bni1*Δ *CDC12/CDC12::URA3::GFP:CDC12*), and into ABY1807 to generate ABY1897 (*tpm1-2 tpm2*Δ *CDC12::URA3::GFP:CDC12*). ABY1897 was mated with ABY1894 (*MAT*α *tpm1-2 tpm2*Δ) to generate ABY1899 (*tpm1-2/tpm1-2 tpm2*Δ*/tpm2*Δ *CDC12/CDC12::URA3::GFP:CDC12*).

For visualization of Bnr1p, one chromosomal copy of *BNR1* in YEF473 (Bi and Pringle, 1996) was COOH-terminally tagged in-frame with *GFP*$^{F64L/S65T}$ by a PCR-based method (Longtine *et al*., 1998). This strain was sporulated and appropriate progeny mated to generate YEF2255 (*BNR1:GFP/BNR1:GFP*). To test for functionality of *BNR1:GFP*, YEF2255 was sporulated to yield haploid ABY1882. This strain was mated to ABY1802 (*bni1*Δ), and the resultant diploid sporulated. No lethality of the progeny was observed, and the *bni1*Δ phenotype of wide necks and rounded buds and the Bnr1pGFP-associated fluorescence segregated 2:2 independently, showing no synthetic growth deficits. However, isolation of the homozygous ABY2256 (*bni1*Δ*/bni1*Δ *BNR1:GFP/BNR1:GFP*) was extremely difficult, even through ABY2256 displayed no growth defect beyond that expected for *bni1*Δ*/bni*Δ cells, and the haploid *bni1*Δ *BNR1:GFP* were able to mate with wild-type cells. Because no similar difficulty had been observed in previously isolating ABY1867, Bnr1pGFP may specifically be defective in supporting mating compared with Bnr1p.

To visualize Bnr1p in conditional tropomyosin mutants, ABY1882 was transformed with *Nde*I/*Kpn*I-linearized pDP116 to generate ABY1885 (*tpm2*Δ*::TRP1 BNR1:GFP*), and then transformed with *BsmAI*/*Bcg*I-linearized pDP115 (Pruyne *et al*., 1998), to generate ABY1886 (*tpm1-2::LEU2 tpm2*Δ*::TRP1 BNR1:GFP*). *TPM2* deletion was confirmed by Western analysis, and *tpm1-2* replacement confirmed by observation of rapid temperature-sensitive cable disassembly and Myo2p delocalization. Diploid ABY1891 (*tpm1-2/tpm1-2 tpm2*Δ*/tpm2*Δ *BNR1:GFP/BNR1:GFP*) was generated by transformation of ABY1886 with YCp50-HO12 mating-type switching plasmid (Russell *et al*., 1986), followed by isolation of HO12-free yeast on 5-fluorootic acid–containing medium.

To visualize Bnr1p in a conditional septin mutant, ABY1637 was mated to ABY1881 (a haploid segregant of YEF2255), and the resultant diploid sporulated. Temperature-sensitive, Kan^R segregants were remated to isolate the homozygous diploid ABY2262 (*cdc10-1/cdc10-1 BNR1:GFP/BNR1:GFP*).

For visualization of *RHO1*, a fusion of *RHO1* upstream DNA sequences (–161 to –1), followed by ATG and a triple hemagglutinin (HA)-tag, followed by the *RHO1* ORF and downstream sequence to +766, followed by *URA3*, followed by further *RHO1* downstream sequence (+767 to +876) was generated by five PCR reactions by using the primer pairs GATCATTCCTCTGAGTATTG and CTTTCTAGTATAATTTTTAAAGTTCTATG (with genomic DNA template), AAAAATTATACTAGAAAGATGGCCTACCCATACGATGTT and GTTACCAACTTGTTGTGACATGCACTGAGCAGCGTAATC (with pCS124 template; kindly provided by C. Shamu, Harvard Medical School, Cambridge, MA), ATGTCACAACAAGTTGGTAAC and CTGGGAGAAAAACAAGT (genomic DNA template), ACTTGTTTTTCTCCCAGGCAGATTGTACTGAGAGTGC and GAATAAGATTATACACATAGATGCGGTATTTTCTCCT (pRS306 template), and TATGTGTATAATCTTATTC and GGATACGCACTTGTAAAT (genomic DNA template), followed by stepwise combination of products by fusion PCR. The final product was transformed into ABY946 (*tpm2*Δ) to replace *RHO1* at the genomic locus, generating ABY1166 (*tpm2*Δ *HA3RHO1::URA3*). Replacement and functionality of *HA3:RHO1* were confirmed by PCR amplification of the *RHO1* locus,

TABLE 1. Yeast strains used in this study

Strain	Genotype	Source
ABY501	*MATa/α ade2-101/ade2-101 his3-Δ200/his3-Δ200 leu2-3,112/leu2-3,112 lys2-801/lys2-801 ura3-52/ura3-52*	Derived from ABY531 (Schott *et al.*, 1999)
ABY506	*MATa/α ade2-101/ade2-101 his3-Δ200/his3-Δ200 leu2-3,112/leu2-3,112 lys2-801/lys2-801 ura3-52/ura3-52 myo2-16::LEU2/myo2-16::HIS3*	Derived from ABY536 (Schott *et al.*, 1999)
ABY944	*MATa his3-Δ200 leu2-3,112 lys2-801 trp1-1(am) ura3-52 tpm1-2::LEU2 tpm2::HIS3*	Pruyne *et al.* (1998)
ABY945	*MATa his3-Δ200 leu2-3,112 lys2-801 trp1-1(am) ura3-52 tpm2::HIS3*	Pruyne *et al.* (1998)
ABY971	*MATa/α his3-Δ200/his3-Δ200 leu2-3,112/leu2-3,112 lys2-801/lys2-801 trp1-1(am)/trp1-1(am) ura3-52/ura3-52 tpm1-2::LEU2/tpm1-2::LEU2 tpm2::HIS3/tpm2::HIS3*	Pruyne *et al.* (1998)
ABY973	*MATa/α his3-Δ200/his3-Δ200 leu2-3,112/leu2-3,112 lys2-801/lys2-801 trp1-1(am)/trp1-1(am) ura3-52/ura3-52 tpm2::HIS3/tpm2::HIS3*	Pruyne *et al.* (1998)
ABY993	*MATa/α his3-Δ200/his3-Δ200 leu2-3,112/leu2-3,112 lys2-801/lys2-801 trp1-1(am)/trp1-1(am) ura3-52/ura3-52 sec6-4/sec6-4*	Derived from EHY52 (Harsay and Schekman, 2002)
ABY994	*MATa/α ura3-52/ura3-52 leu2-3,112::SEC8:3×-c-myc::LEU2/leu2-3,112::SEC8:3×-c-myc::LEU2 sec4-8/sec4-8*	Derived from NY1373 (Finger *et al.*, 1998)
ABY995	*MATa/α ura3-52/ura3-52 leu2-3,112::SEC8:3×-c-myc::LEU2/leu2-3,112::SEC8:3×-c-myc::LEU2 sec10-2/sec10-2*	Derived from NY1389 (Finger *et al.*, 1998)
ABY996	*MATa/α ura3-52/ura3-52 leu2-3,112::SEC8:3×-c-myc::LEU2/leu2-3,112::SEC8:3×-c-myc::LEU2 sec15-1/sec15-1*	Derived from NY1390 (Finger *et al.*, 1998)
ABY1166	*MATα his3-Δ200 leu2-3,112 lys2-801 trp1-1(am) ura3-52 tpm2::HIS3 3×-HA:RHO1::URA3*	This study
ABY1171	*MATa/α his3-Δ200/his3-Δ200 leu2-3,112/leu2-3,112 lys2-801/lys2-801 trp1-1(am)/trp1-1(am) ura3-52::ACT1promoter:GFP^{S65T}:BUD6::URA3/ura3-52::ACT1promoter:GFP^{S65T}:BUD6::URA3 tpm1-2::LEU2/tpm1-2::LEU2 tpm2::HIS3/tpm2::HIS3 SEC8:3×-HA::TRP1/SEC8:3×-HA::TRP1*	This study
ABY1197	*MATa/α his3-Δ200/his3-Δ200 leu2-3,112/leu2-3,112 lys2–801/lys2-801 trp1-1(am)/trp1-1(am) ura3-52::SPA2:GFP^{S65T}::URA3/ura3-52::SPA2:GFP^{S65T}::URA3*	This study
ABY1198	*MATa/α his3-Δ200/his3-Δ200 leu2-3,112/leu2-3,112 lys2-801/lys2-801 trp1-1(am)/trp1-1(am) ura3-52::SPA2^{S65T}:GFP::URA3/ura3-52::SPA2:GFP^{S65T}::URA3 tpm2::HIS3/tpm2::HIS3*	This study
ABY1199	*MATa/α his3-Δ200/his3-Δ200 leu2-3,112/leu2-3,112 lys2-801/lys2-801 trp1-1(am)/trp1-1(am) ura3-52::ACT1promoter:GFP^{S65T}:BUD6::URA3/ura3-52::ACT1promoter:GFP^{S65T}:BUD6::URA3 tpm2::HIS3/tpm2::HIS3*	This study
ABY1601	*MATa/α his3-Δ200/his3-Δ200 leu2-3,112/leu2-3,112 lys2-801/lys2-801 trp1-1(am)/trp1-1(am) ura3-52/ura3-52 tpm2::HIS3/tpm2::HIS3 3×-HA:RHO1::URA3/3×-HA:RHO1::URA3*	This study
ABY1602	*MATa/α his3-Δ200/his3-Δ200 leu2-3,112/leu2-3,112 lys2-801/lys2-801 trp1-1(am)/trp1-1(am ura3-52/ura3-52 tpm1-2::LEU2/tpm1-2::LEU2 tpm2::HIS3/tpm2::HIS3 3×-HA:RHO1::URA3/3×-HA:RHO1::URA3*	This study
ABY1637	*MATa his3-Δ200 leu2-3,112 lys2-801 trp1-1(am) ura3-52 tpm2::HIS3 cdc10-1*	This study
ABY1638	*MATα his3-Δ200 leu2-3,112 lys2-801 trp1-1(am) ura3-52 tpm2::HIS3 cdc10-1*	This study
ABY1639	*MATa his3-Δ200 leu2-3,112 trp1-1(am) ura3-52 tpm1-2::LEU2 tpm2::HIS3 cdc10-1*	This study
ABY1641	*MATa his3-Δ200 leu2-3,112 lys2-801 trp1-1(am) ura3-52 tpm2::HIS3 cdc12-6*	This study
ABY1643	*MATa his3-Δ200 leu2-3,112 lys2-801 trp1-1(am) ura3-52 tpm1-2::LEU2 tpm2::HIS3 cdc12-6*	This study
ABY1662	*MATa/α his3-Δ200/his3-Δ200 leu2-3,112/leu2-3,112 lys2-801/lys2-801 trp1-1(am)/trp1-1(am) ura3-52/ura3-52 tpm2::HIS3/tpm2::HIS3 cdc10-1/cdc10-1*	This study
ABY1665	*MATa/α his3? his4? leu2-3,112/leu2-3,112 lys2-801/lys2-801 trp1-1(am)/trp1-1(am) tpm2::HIS3/tpm2::HIS3 sec2-41/sec2-41*	This study
ABY1801	*MATa/α his3Δ1/his3Δ1 met15? leu2Δ0/leu2Δ0 lys2? ura3Δ0/ura3Δ0 bnr1Δ::Kan^R/bnr1Δ::Kan^R*	Evangelista *et al.* (2002)
ABY1802	*MATα his3Δ0 leu2Δ0 lys2Δ0 ura3Δ0 bni1Δ::Kan^R*	Evangelista *et al.* (2002)
ABY1803	*MATa/α his3Δ1/his3Δ1 met15? leu2Δ0/leu2Δ0 lys2? ura3Δ0/ura3Δ0 bni1-11::URA3/bni1-11::URA3 bnr1Δ::Kan^R/bnr1Δ::Kan^R*	Evangelista *et al.* (2002)
ABY1804	*MATα his3Δ leu2 lys2 trp1? ura3 tpm1-2:LEU2 tpm2::HIS3 bnr1Δ::Kan^R*	Evangelista *et al.* (2002)
ABY1805	*MATα his3Δ leu2 lys2 trp1-1(am) ura3 tpm1-2::LEU2 tpm2::HIS3 bni1-12::URA3*	Evangelista *et al.*, 2002
ABY1806	*MATα his3Δ leu2 lys2 trp1? ura3 tpm1-2::LEU2 tpm2::HIS3 bni1-12::URA3 bnr1Δ::Kan^R*	Evangelista *et al.* (2002)

TABLE 1. Continued

Strain	Genotype	Source
ABY1807	*MATa his3Δ1 met15Δ0 leu2Δ0 ura3Δ0 tpm1-2::LEU2 tpm2Δ::Kan^R*	Evangelista *et al.* (2002)
ABY1810	*MATa his3Δ1 met15Δ0 leu2Δ0 ura3Δ0 spa2Δ::Kan^R*	Evangelista *et al.* (2002)
ABY1848	*MATa/α his3Δ1/his3Δ1 met15Δ0/MET15 leu2Δ0/leu2Δ0 lys2Δ0/LYS2 ura3Δ0/ura3Δ0*	Evangelista *et al.* (2002)
ABY1867	*MATa/α his3Δ1/his3Δ1 met15Δ0/MET15 leu2Δ0/leu2Δ0 lys2Δ0/LYS2 ura3Δ0/ura3Δ0 bni1Δ::Kan^R/bni1Δ::Kan^R*	Evangelista *et al.* (2002)
ABY1882	*MATα his3 leu2 lys2 trp1 ura3 BNR1:GFP$^{F64L/S65T}$::Kan^R*	This study
ABY1882	*MATa his3 leu2 lys2 trp1 ura3 BNR1:GFP$^{F64L/S65T}$::Kan^R*	This study
ABY1885	*MATa his3 leu2 lys2 trp1 ura3 tpm2Δ::TRP1 BNR1:GFP$^{F64L/S65T}$::Kan^R*	This study
ABY1886	*MATa his3 leu2 lys2 trp1 ura3 tpm1-2::LEU2 tpm2Δ::TRP1 BNR1:GFP$^{F64L/S65T}$::Kan^R*	This study
ABY1891	*MATa/α his3/his3 leu2/leu2 lys2/lys2 trp1/trp1 ura3/ura3 tpm1-2::LEU2/tpm1-2::LEU2 tpm2Δ::TRP1/tpm2Δ::TRP1*	This study
ABY1894	*MATα his3Δ1 leu2Δ0 ura3Δ0 tpm1-2::LEU2 tpm2Δ::Kan^R*	This study
ABY1896	*MATa/α his3Δ1/his3Δ1 met15Δ0/MET15 leu2Δ0/leu2Δ0 lys2Δ0/LYS2 ura3Δ0/ura3Δ0 CDC12::URA3::GFP:CDC12/CDC12*	This study
ABY1897	*MATa his3Δ1 met15Δ0 leu2Δ0 ura3Δ0 tpm1-2::LEU2 tpm2Δ::Kan^R CDC12::URA3::GFP:CDC12*	This study
ABY1898	*MATa/α his3Δ1/his3Δ1 met15Δ0/MET15 leu2Δ0/leu2Δ0 lys2Δ0/LYS2 ura3Δ0/ura3Δ0 bni1Δ::Kan^R/bni1Δ::Kan^R CDC12::URA3::GFP:CDC12/CDC12*	This study
ABY1899	*MATa/α his3Δ1/his3Δ1 met15Δ0/MET15 leu2Δ0/leu2Δ0 ura3Δ0/ura3Δ0 tpm1-2::LEU2/tpm1-2::LEU2 tpm2Δ::Kan^R/tpm2Δ::Kan^R CDC12::URA3::GFP:CDC12/CDC12*	This study
ABY2000	*MATα his3Δ1 leu2Δ0 lys2Δ0 ura3Δ0 bni1-11::ura3Δ::HIS3 bnr1Δ::Kan^R*	This study
ABY2201	*MATa his3 leu2 lys2 ura3 tpm2::HIS3 cdc10-1*	This study
ABY2209	*MATα his3 leu2 lys2 ura3 bni1-11::URA3*	This study
ABY2218	*MATα his3 leu2 lys2 ura3 bni1-11::URA3 bnr1Δ::Kan^R*	This study
ABY2226	*MATa his3 leu2 lys2 ura3 trp1-1(am) bni1-11::URA3 cdc10-1*	This study
ABY2247	*MATa/α his3/his3 leu2/leu2 lys2/lys2 ura3/ura3 tpm2::HIS3/tpm2::HIS3 bni1-11::URA3/bni1-11::URA3*	This study
ABY2250	*MATa/α his3Δ1/his3Δ1 met15Δ0/MET15 leu2Δ0/leu2Δ0 lys2Δ0/LYS2 ura3Δ0/ura3Δ0 tpm1-2::LEU2/tpm1-2::LEU2 tpm2Δ::Kan^R/tpm2Δ::Kan^R*	This study
ABY2251	*MATα his3Δ1 leu2Δ0 met15Δ0 ura3Δ0 CLN2::URA3::GAL1-10:CLN2*	This study
ABY2252	*MATα his3Δ1 leu2Δ0 met15Δ0 ura3Δ0 tpm1-2::LEU2 tpm2Δ::Kan^R CLN2::URA3::GAL1-10:CLN2*	This study
ABY2256	*MATa/α his3/his3 leu2/leu2 lys2/lys2 trp1/trp1 ura3/ura3 bni1Δ::Kan^R/bni1Δ::Kan^R BNR1:GFP$^{F64L/S65T}$::Kan^R/BNR1:GFP$^{F64L/S65T}$:Kan^R*	This study
ABY2257	*MATa/α his3-Δ200/his3-Δ200 leu2-3,112/leu2-3,112 lys2-801/lys2-801 trp1-1(am)/trp1-1(am) ura3-52/ura3-52 tpm2::HIS3/tpm2::HIS3 cdc10-1/cdc10-1 CDC12/CDC12::URA3::GFP:CDC12*	This study
ABY2262	*MATa/α his3/his3 leu2/leu2 lys2/lys2 trp1/trp1 ura3/ura3 BNR1:GFP$^{F64L/S65T}$::Kan^R/BNR1:GFP$^{F64L/S65T}$:Kan^R cdc10-1/cdc10-1*	This study
NY132	*MATα his4-619 ura3-52 sec2-41*	Novick *et al.* (1980)
RSY255	*MATα leu2-3,112 ura3-52*	Kaiser and Schekman (1990)
RSY267	*MATα his4-619 ura3-52 sec16-2*	Kaiser and Schekman (1990)
RSY281	*MATα his4-619 ura3-52 sec23-1*	Kaiser and Schekman (1990)
Y1239	*MATa his3Δ1 leu2Δ0 met15Δ0 ura3Δ0*	Evangelista *et al.* (2002)
Y4133	*MATa his3Δ1 leu2Δ0 met15Δ0 ura3Δ0 bni1-11::URA3 bnr1Δ::Kan^R*	Evangelista *et al.* (2002)
YEF2255	*MATa/α his3/his3 leu2/leu2 lys2/lys2 trp1/trp1 ura3/ura3 BNR1:GFP$^{F64L/S65T}$::Kan^R/BNR1:GFP$^{F64L/S65T}$:Kan^R*	This study

sequencing of the *RHO1* ORF, demonstration of normal morphology at 18 and 37°C, normal polarization of Myo2p at 18 and 34.5°C, and normal Myo2p depolarization at 38°C. Through mating ABY1166 with ABY944, followed by sporulation and mating of progeny, ABY1601 (*tpm2Δ/tpm2Δ HA3RHO1/HA3RHO1*) and ABY1602 (*tpm1-2/tpm1-2 tpm2Δ/tpm2Δ HA3RHO1/HA3RHO1*) were isolated.

For ease of immunofluorescence imaging, previously described haploid *myo2* and *sec* strains were converted to diploids (Table 1). ABY1665 (*sec2-41/sec2-41 tpm2Δ/tpm2Δ*) was obtained through crossing of ABY945 and NY132 (*sec2-41*) and subsequent sporulation and mating of progeny.

Production of GSTBnr1p(FH1FH2) Recombinant Protein

Protease-deficient bacterial strain ER2508 (New England Biolabs, Beverly, MA) was transformed with either pGEX-6P-3 or p080 and grown in 2-liter culture at 30°C to OD_{600} = 1.0 before induction with 1 mM isopropyl β-D-thiogalactoside for 3 h at 30°C. Cultures were resuspended in GST-buffer A (20 mM Tris-HCl, pH 7.4, 0.2 mM EDTA, 1 M NaCl) with 1 mM dithiothreitol (DTT) and protease inhibitor cocktail (Sigma-Aldrich, St. Louis, MO), and then sonicated. High-speed supernatants were incubated against glutathione-agarose (Sigma-Aldrich), washed, and eluted in GST-buffer C (20 mM Tris-HCl, pH 7.4, 0.02 mM EDTA, 0.1 M NaCl, 5 mM reduced glutathione).

Pyrene-Actin Polymerization Assays

Equal amounts of purified rabbit muscle actin (purified as described by MacLean-Fletcher and Pollard, 1980) and pyrene rabbit muscle actin (Cytoskeleton, Denver, CO) were combined in G-buffer (10 mM Tris-HCl, pH 7.5, 0.2 mM $MgCl_2$, 1 mM DTT, 0.5 mM ATP) and precleared at 180,000 × g for 100 min at 4°C before use. Varying concentrations of GST or GSTBnr1p(FH1FH2) were combined with 3 μM actin and polymerization was induced by addition of F-buffer (giving final concentrations of 0.5 mM ATP, 5 mM $MgCl_2$, 12.5 mM KCl). Pyrene fluorescence at 407 nm was monitored

under excitation at 365 nm with a model 814 photomultiplier detection system (Photon Technology International, Monmouth Junction, NJ).

Generation of Bni1p-specific Antibodies

A GST-fusion protein containing the Bni1p residues 1227–1953 was expressed from p4565 in BL21 *Escherichia coli* and purified as described previously (Pruyne *et al*., 2002). Protein was resolved by SDS-PAGE, excised, eluted, and dialyzed against phosphate-buffered saline (PBS), yielding 3 μg of protein for injection into two rabbits. Collected antiserum from one rabbit diluted 1:2000 recognized a 9E10 (anti-*myc*) reactive band on a blot of yeast extract producing Bni1p-*myc* (Evangelista *et al*., 2002), which was absent from noninduced yeast extract and which was not recognized by preimmune serum. Affinity-purified serum was produced by incubation of crude serum with GST-Bni1p (1227–1953) CNBr-coupled to Sepharose beads (Sigma-Aldrich), followed by elution with 0.1 M glycine-HCl, pH 2.5, and buffering to pH 7.4 with unbuffered 1 M Tris. Immunofluorescence of cells overexpressing Bni1p-*myc* showed complete costaining of anti-Bni1p and 9E10. Wild-type and *bni1*Δ yeast showed diffuse cytoplasmic staining and a faint nuclear stain, but only wild-type cells showed a polarized stain characteristic of Bni1p.

Light Microscopy and Imaging

Immunofluorescence microscopy for Tpm1p, Myo2p, HA epitope, and Cdc42p was performed as described previously (Pruyne *et al*., 1998; Kozminski *et al*., 2000). Immunofluorescence staining for GFP-fusions of Bud6p, Cdc12p, and Spa2p by using GFP-specific antibodies (kindly provided by P. Silver, Dana-Farber Cancer Institute, Boston, MA) was performed in the same manner, with the primary antibodies diluted 1:250 in PBS/1% bovine serum albumin. Anti-Bni1p staining or anti-GFP staining for Bnr1pGFP required 30-min fixation, and 3-h incubation with primary antibodies. Anti-Bni1p was diluted 1:30. Cells were observed on an Axiovert 100 TV microscope (Carl Zeiss, Thornwood, NY), and images were captured through using an RTE (round thermoelectric passive)/charge-coupled device (CCD) digital camera (Princeton Scientific Instruments, Monmouth Junction, NJ), and processed using the MetaMorph Imaging System (Universal Imaging, Downingtown, PA).

For fluorescence microscopy of Bni1pGFP, Bnr1pGFP, or GFPCdc12p in fixed cells, yeast were fixed for 30 s by direct addition of 37% HCHO to a final concentration of 5%, and then washed twice in equal volumes of PBS and resuspended in 1/10 volume of PBS. Images were acquired and processed as for immunofluorescence.

For live cell fluorescence microscopy of cells expressing GFPSec4p, Bni1pGFP, or Spa2pGFP, cells were mounted on 2% agarose containing standard synthetic complete medium and observed at 22°C under on a Nikon eclipse TE-2000U microscope (Nikon, Tokyo, Japan) by using the UltraVIEW LCI confocal imaging system (PerkinElmer Life and Analytical Sciences, Boston, MA). Movies of single focal planes were acquired through consecutive 80-ms exposures by using a C4742-95-12ERG 12-bit digital output CCD camera (Hamamatsu Photonics, Bridgewater, NJ). All still images presented were processed nonlinearly through Adobe Photoshop (Adobe Systems, Mountain View, CA) to reduce background haze but preserve faint structures.

Assays for Scoring Cytoskeletal Organization and Membrane Trafficking

For indicated assays, yeast cells were visually assigned as unbudded, small-budded (bud length $<1/3$ mother cell length), medium-budded ($1/3$ mother cell length $\leq$ bud length $<2/3$ mother cell length), or large-budded (bud length $\geq 2/3$ mother cell length). For scoring the distribution of actin cables in unbudded cells, cells treated for Tpm1p immunofluorescence were visually scored for the presence or absence of cables associated with a single point on the cell cortex. For assessing actin cable distribution for cells of other budding categories were visually scored based on whether Tpm1p displayed a strong stain in the bud, a strong association with cables that intersected the bud neck, a combination of the two, or neither.

For assessing the location of actin cable assembly or the location of Myo2p, Bni1p, HARho1p, GFPBud6p, Spa2pGFP, Cdc42p, Bnr1pGFP, or GFPCdc12p in budded cells, cells of the appropriate budding categories stained for the appropriate epitope were visually scored based on whether the stain was concentrated over background levels at the bud tip, in puncta along the bud cortex, at the bud neck, at a combination of the bud tip and neck, or at none of these. For assessing the distribution of any of these markers except GFPCdc12p in unbudded cells, cells were scored based on whether the stain was localized to a single point on the cell cortex or was delocalized. GFPCdc12p localization in unbudded cells was categorized as either associated with a large ring indicative of a cytokinetic remnant, with a small patch or ring presumed to reflect the nascent bud site, with both structures, or with neither.

For scoring GFPSec4p-associated particle density, movies of 19 small- or medium-budded cells of each strain acquired at a focal plane containing the bud neck were examined frame-by-frame by using QuickTime Player (Apple Computer, Cupertino, CA). The mother cells were visually divided into halves near or away from the bud. The number of discrete GFPSec4p-associated particles in each half was counted every 2 s over the 40-s movies. True fluorescent particles were discriminated from noise by observation of three successive movie frames (encompassing ~0.24 s), with fluorescent bodies in-focus in at least one frame and present in at least two consecutive frames being considered true particles. Cell areas were determined by importing a representative frame from each movie into MetaMorph Imaging System (Universal Imaging) and measuring the area in pixels, with cell areas calculated based on the TIF pixels corresponding to a calculated 0.00416 μm^2 based on a 6.45 $\times$ 6.45-μm camera pixel size and use of a 100$\times$ objective.

For scoring the likelihood of GFPSec4p-associated particles to undergo directed movements, movies of 23 wild-type, 25 *bnr1*Δ/*bnr1*Δ, and 19 *bni1*Δ/*bni1*Δ were observed for 5-s intervals, and fluorescent particles were scored as positive if seen to commence movement along a single straight or curved trajectory for $\geq 1/3$ the mother cell length over four consecutive frames, and as negative if they disappeared or exhibited only random motions.

RESULTS

Bni1p and Bnr1p Maintain Distinct Sets of Actin Cables

Although Bni1p and Bnr1p show partial redundancy with each other for actin cable assembly, only Bni1p has been shown to stimulate actin assembly in vitro or in vivo. In the absence of regulatory NH_2-terminal sequences, overexpression of the Bni1p FH1 and FH2 domains in yeast stimulates assembly of cable-like filaments (Evangelista *et al*., 1997, 2002). To determine whether Bnr1p exhibits the same properties, we overexpressed NH_2-terminally truncated Bnr1p (residues 386-1375) in wild-type cells and stained for actin (Act1p) distribution by immunofluorescence microscopy. Cells expressing this Bnr1p construct showed an overabundance of actin within the bud to the degree that discrete cortical actin patches were no longer visible, just as occurs with overexpression of NH_2-terminally truncated Bni1p (Figure 1A), indicating the Bnr1p COOH-terminal region, including the FH1 and FH2 domains can stimulate the assembly of cable-like filaments in vivo.

In vitro, the Bni1p FH2 domain can nucleate actin filaments from monomers, with the FH1 enhancing the efficiency of this reaction (Pruyne *et al*., 2002; Sagot *et al*., 2002b). To determine whether the Bnr1p FH1 and FH2 domains also nucleate actin filaments in vitro, a recombinant GST-fusion construct encompassing the Bnr1p FH1 and FH2 domains plus COOH-terminal sequences (residues 757-1375) was examined for the ability to accelerate the assembly of pyrene-conjugated actin (Figure 1B). As has been seen for similar Bni1p-derived constructs, this construct stimulated the polymerization of actin from monomers, whereas GST did not. Thus, the conserved COOH-terminal regions of the two yeast formins stimulate actin assembly.

Based on studies of overexpressed Bni1p and Bnr1p, the NH_2 termini of these formins help confer distinct localizations on the two (Jansen *et al*., 1996; Evangelista *et al*., 1997; Fujiwara *et al*., 1998; Kamei *et al*., 1998; Ozaki-Kuroda *et al*., 2001). We wished to examine whether these localizations impart differences in the distribution of the actin filaments assembled by the two isoforms. However, overexpression of either formin alters actin organization and cell morphology (Kamei *et al*., 1998; Evangelista *et al*., 2002; Sagot *et al*., 2002a). To avoid this complication, we observed the distribution of the formins and formin-dependent actin filaments in cells that expressed Bni1p and Bnr1p at endogenous levels.

Immunofluorescence staining of endogenous Bni1p agreed with the reported distribution for overexpressed epitope-tagged Bni1p, concentrating at the nascent bud sites of unbudded cells, at the tips of small buds, in a crescent over the surfaces of medium buds, and at the septal planes between dividing cells (Figures 1C and S1A). A COOH-terminal GFP-fusion of full-length Bnr1p expressed from the *BNR1* locus also displayed a localization in agreement with

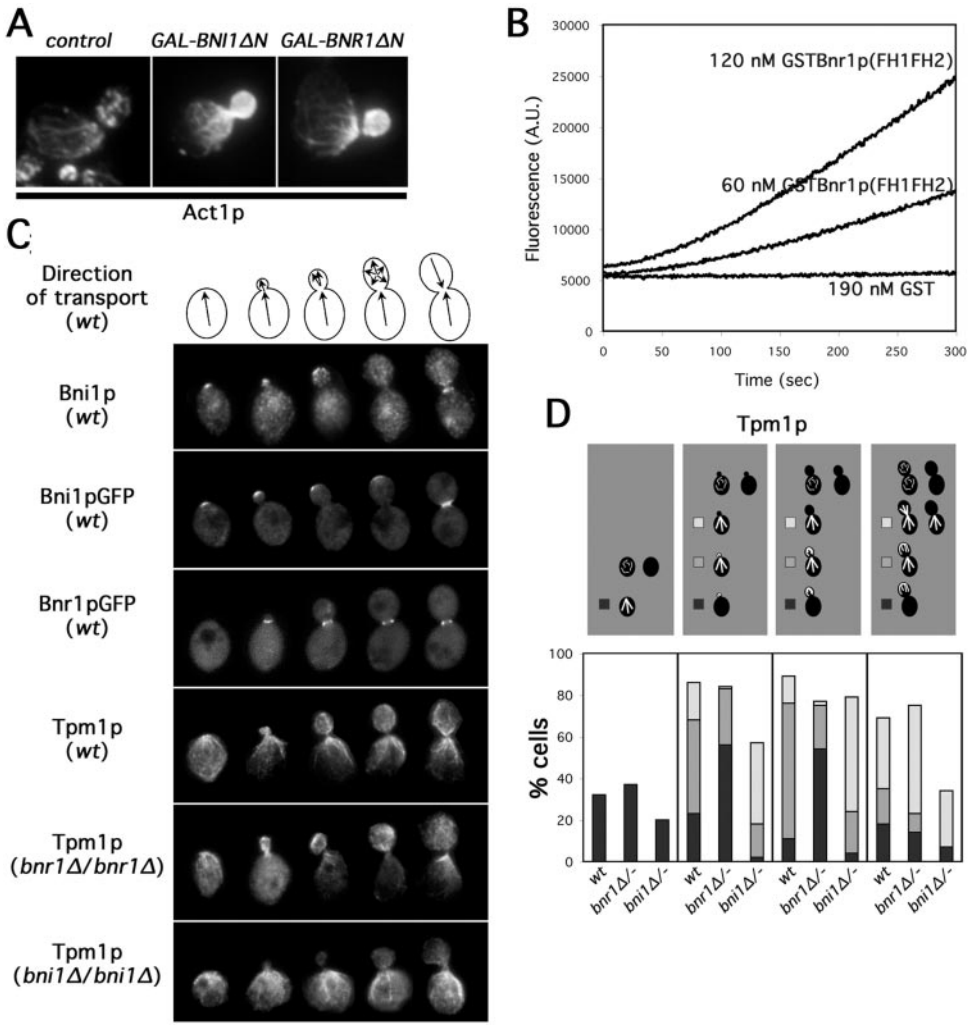

Figure 1. Bni1p and Bnr1p are important for distinct sets of actin cables. (A) Wild-type cells (Y1239) were grown 2 h in galactose to induce a control vector or NH_2-terminally truncated Bni1p (*BNI1*Δ*N*) or Bnr1p (*BNR1*Δ*N*) and stained for Act1p distribution by immunofluorescence microscopy. (B) Recombinant GST (190 nM) or GSTBnr1p(FH1FH2) (60 or 120 nM) were combined with 3 μM G-actin (~5% pyrene labeled), and actin assembly was monitored through increases in pyrene fluorescence (measured in arbitrary units). (C) Models depict the direction of polarized transport in yeast at various stages of bud growth that correspond with cell images below. Bni1p is shown in selected wild-type cells (ABY1848) treated for anti-Bni1p immunofluorescence or expressing Bni1pGFP from a high-copy plasmid. Bnr1pGFP fluorescence is shown in selected wild-type cells (YEF2255). The distribution of actin cables in selected wild-type (ABY1848), *bnr1*Δ/*bnr1*Δ (ABY1801), and *bni1*Δ/*bni1*Δ (ABY1867) cells is shown by anti-Tpm1p immunofluorescence microscopy. (D) One hundred cells of each indicated budding categories of wild-type (ABY1848), *bnr1*Δ/*bnr1*Δ (ABY1801), and *bni1*Δ/*bni1*Δ (ABY1867) strains were processed for localization of Tpm1p by immunofluorescence microscopy as a reporter for actin cable organization. Unbudded cells scored as either having organized cables (black) or disorganized cables (blank). Budded cells were categorized as having unorganized cables (blank), cables predominantly associated with the bud cortex (black), cables associated with bud cortex and neck (gray), or cables predominantly associated with the bud neck (white).

previous overexpression studies (Kamei *et al*., 1998), showing a polarized distribution in very few unbudded cells (5% of unbudded cells), but a ring of fluorescence around the neck of cells with buds of all sizes (Figures 1C and S1A).

In yeast, formin-dependent actin filaments can be distinguished from the Arp2/3 complex-dependent filaments by their association with the F-actin binding protein tropomyosin, encoded by the *TPM1* and *TPM2* genes (Liu and Bretscher, 1989; Pruyne *et al*., 1998; Evangelista *et al*., 2002; Sagot *et al*., 2002a; Tolliday *et al*., 2002). To determine whether Bni1p or Bnr1p make distinct contributions to assembling these filaments, we examined Tpm1p distribution in wild-type yeast and strains lacking Bni1p (*bni1*Δ/*bni1*Δ) or Bnr1p (*bnr1*Δ/*bnr1*Δ) (Figure 1, C and D). Importantly, for both deletion strains, the localization of the remaining formin isoform was not perturbed compared with wild-type cells (Figure S1A and B).

In asynchronous wild-type cultures, unbudded cells are either undergoing depolarized growth or bud initiation, and thus, Tpm1p was present in either disorganized cables or cables radiating from the nascent bud site. Unbudded *bnr1*Δ/*bnr1*Δ cells showed a similar distribution as wild-type yeast, whereas unbudded *bni1*Δ/*bni1*Δ cells displayed a higher incidence of unorganized cables, and when filaments were organized, they formed a patch at one pole rather than an array of cables (Figure 1, C and D). Thus, Bni1p, which is polarized in unbudded cells, is important for organizing actin cables in these cells, whereas Bnr1p, which is largely depolarized in these cells, is not important for this.

Cells with small- and medium-sized buds are undergoing bud growth. In wild-type cells, Tpm1p-stained cables formed a meshwork in the bud that was concentrated at the tip, and an array that radiated from the bud neck into the mother cell (Figure 1, C and D). In *bnr1*Δ/*bnr1*Δ cells, the cable meshwork in the bud was present, but the proportion of cells with prominent cables in the mother (Figure 1D, gray + white bars) was reduced from 76% of wild-type cells to 25% of *bnr1*Δ/*bnr1*Δ cells. In contrast, cables were prominent in *bni1*Δ/*bni1*Δ mother cells, but the percentage with Tpm1p stain in the bud (Figure 1D, gray + black bars) was reduced from 72% of wild-type cells to 21% of *bni1*Δ/*bni1*Δ cells. Thus, there are correlations between bud-associated cables and Bni1p activity and between neck-associated cables and Bnr1p activity.

Large-budded cells are either continuing bud growth, undergoing cytokinesis, or depositing new cell wall between divided cells. Thus, Tpm1p-staining in wild-type cells either resembled small- and medium-budded cells, labeled a contractile ring around the neck plus disorganized cables, or

labeled cables radiating from the septal plane into the mother and daughter cells (Figure 1, C and D). Both formins support the assembly of the contractile ring (Vallen *et al*., 2000), so we did not examine that structure. Cables in *bnr1*Δ/*bnr1*Δ cells were similar to wild-type yeast, but they were more likely to be disorganized in *bni1*Δ/*bni1*Δ cells (Figure 1, C and D).

These results show that Bni1p and Bnr1p have distinct functions in organizing actin cables. Although the two formins show some ability to compensate for the loss of the other isoform (Figure 1D), Bni1p shows a strong preference for maintaining cables at the nascent bud site and along the growing bud cortex, whereas Bnr1p shows a strong preference for maintaining neck-associated cables in the mother during bud growth.

Yeast Lacking Bni1p or Bnr1p Exhibit Myosin-V Transport Defects

The myosin-V Myo2p rapidly translocates along actin cables to concentrate at growth sites (Johnston *et al*., 1991; Lillie and Brown, 1994; Pruyne *et al*., 1998; Schott *et al*., 2002). We examined the distribution of Myo2p in wild-type, *bni1*Δ/*bni1*Δ, and *bnr1*Δ/*bnr1*Δ cells by immunofluorescence staining (Figure 2, A and B). For unbudded cells of all three types, Myo2p localized to a patch that presumably marked the nascent bud site. For all three, the proportion of cells with Myo2p was greater than the proportion that showed polarized cables (Figure 1D), which we believe reflects the greater ease at detecting a single spot of Myo2p than resolving the overall organization of cables that extend throughout the cell. Consistent with the poor organization of actin cables in unbudded *bni1*Δ/*bni1*Δ yeast compared with wild-type or *bnr1*Δ/*bnr1*Δ yeast, unbudded *bni1*Δ/*bni1*Δ cells showed a reduced proportion of cells with properly organized Myo2p compared with the other two strains (Figure 2B). In wild-type and *bnr1*Δ/*bnr1*Δ cells, Myo2p also associated with the growing bud tip and the septal plane of dividing cells, but in *bni1*Δ/*bni1*Δ cells with buds, Myo2p localized to the bud neck and diffusely over the bud cortex, but almost never concentrated at the bud tip (Figure 2, A and B).

Myo2p polarizes growth by delivering secretory vesicles along actin cables (Johnston *et al*., 1991; Walch-Solimena *et al*., 1997; Pruyne *et al*., 1998; Schott *et al*., 1999). The in vivo movement and distribution of vesicles can be observed using a GFP-tagged secretory vesicle-associated rab-GTPase Sec4p (Goud *et al*., 1988; Mulholland *et al*., 1997; Walch-Solimena *et al*., 1997; Schott *et al*., 2002). GFPSec4p occurs in large fluorescent masses within yeast cells, as well as discrete fluorescent particles in the mother cell. The large masses are interpreted to correspond to the cluster of post-Golgi secretory vesicles accumulated at growth sites as seen by electron microscopy, whereas the discrete particles are interpreted to be individual or small clusters of vesicles (Schott *et al*., 2002).

We expressed GFPSec4p in wild-type, *bni1*Δ/*bni1*Δ, and *bnr1*Δ/*bnr1*Δ yeast, and observed living cells (for sample 12-s movies, see Mov. S1–3). GFPSec4p accumulated at the bud tips of small- and medium-budded wild-type and *bnr1*Δ/*bnr1*Δ cells, whereas in *bni1*Δ/*bni1*Δ cells, GFPSec4p concentrated at the bud neck, with a more diffuse accumulation over the bud cortex, consistent with the Myo2p distribution in these cells (Figure 3A). When the discrete particles in the mother cell were examined for each strain, we found that in the half of the mother cell closer to the bud neck, wild-type yeast displayed an average density of 0.06 vesicles/μm^2 (with a SD of 0.08 vesicles/μm^2), *bni1*Δ/*bni1*Δ yeast showed 0.10 ± 0.11 vesicles/μm^2, and *bnr1*Δ/*bnr1*Δ cells showed

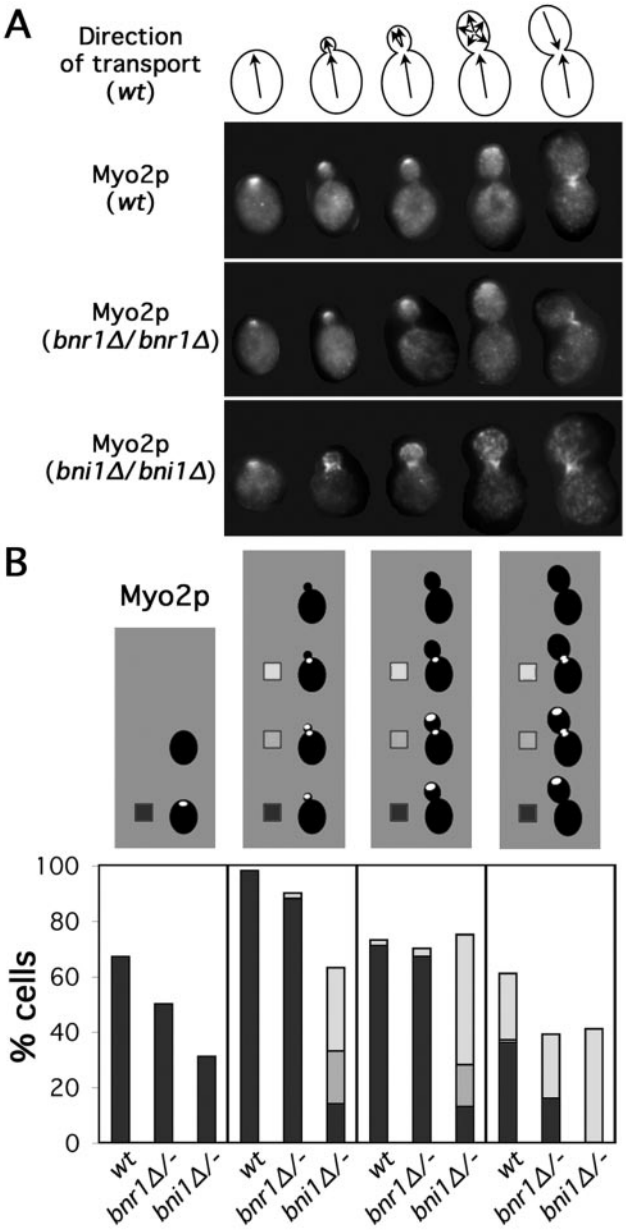

Figure 2. Myo2p localization is perturbed in *bni1*Δ cells. (A) Models as in Figure 1A are depicted with selected wild-type (ABY1848), *bnr1*Δ/*bnr1*Δ (ABY1801), and *bni1*Δ/*bni1*Δ (ABY1867) cells stained to show Myo2p distribution. (B) One hundred cells of each budding category treated as described in A were scored for Myo2p localization. Unbudded cells were categorized as having Myo2p delocalized (blank) or localized to one site on the cell surface (black). Budded cells were scored as having Myo2p localized to the bud cortex (though not necessarily the bud tip) (black), the bud cortex and neck (gray), localized to the bud neck (white), or delocalized (blank).

0.17 ± 0.13 vesicles/μm^2 (315 observations for each strain). When the density of discrete GFPSec4p-associated particles in the half of the mother cell further from the bud neck was examined, wild-type cells showed 0.07 ± 0.08 vesicles/μm^2, *bni1*Δ/*bni1*Δ showed 0.10 ± 0.10 vesicles/μm^2, and *bnr1*Δ/*bnr*Δ showed 0.25 ± 0.20 vesicles/μm^2 (315 observations for each strain). Thus, *bnr1*Δ/*bnr1*Δ cells tended to have an increased number of visible vesicles dispersed in the mother

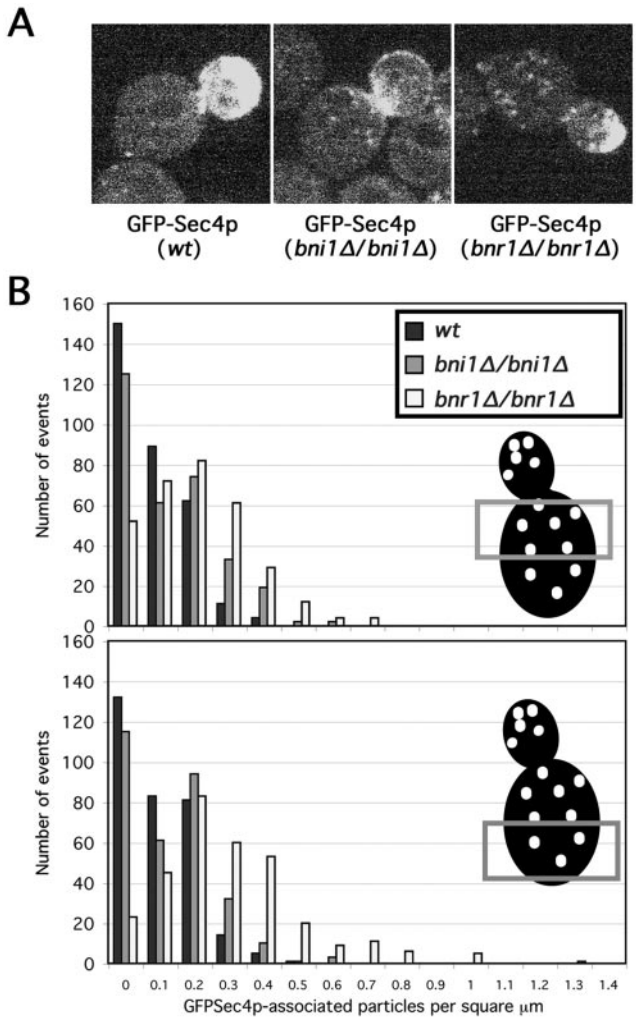

Figure 3. *Bni1*Δ and *bnr1*Δ yeast have unique perturbations in vesicle dynamics. (A) Still GFPSec4p fluorescence images from movies of living wild-type (ABY1848; Mov. S1), *bni1*Δ/*bni1*Δ (ABY1867; Mov. S2), and *bnr1*Δ/*bnr1*Δ (ABY1801; Mov. S3) cells are shown. (B) Results of density counts for individual fluorescent particles from individual frames from 19 movies of GFPSec4p-expressing small- or medium-budded cells of each strain in A are summarized. The density of discrete particles counted in the indicated portions of each mother cell was plotted against the number of times that density was counted (with 315 total counting events for mother cell-half for each strain).

cell compared with *BNR1*+ strains, particularly in the region further from the bud neck (Figure 3, A and B).

The discrete GFPSec4p-associated particles alternatively undergo Brownian motion or Myo2p-dependent directed movements (Schott *et al*., 2002). We examined whether the three yeast strains exhibited different tendencies in the behavior of the fluorescent particles. When small- and medium-budded cells were examined for 5-s intervals, GFPSec4p-associated particles had a 24% chance to engage in directed movements in wild-type cells (71 of 270 observations), 29% chance in *bni1*Δ/*bni1*Δ cells (147 of 500 observations), but only 10% chance in *bnr1*Δ/*bnr1*Δ cells (96 of 920 observations). For wild-type and *bnr1*Δ/*bnr1*Δ cells, these directed movements were from the mother cell into the bud, whereas for *bni1*Δ/*bni1*Δ cells, 17% of directed movements were away from the bud, suggesting some cables were misoriented. These results together indicate Bnr1p promotes efficient engagement of Myo2p-associated cargoes in directed transport in the mother cell, whereas Bni1p promotes Myo2p-dependent traffic from the bud neck to the bud tip.

Formin-stimulated Filament Assembly Occurs at the Bud Cortex and Neck

The ability of formins to stimulate actin assembly in vitro suggests that formin-rich regions of the cell might correspond with cable filament assembly sites. Consistent with this, actin cables decorated in vivo with a GFPAbp140p fusion protein show that new material incorporates into cables somewhere near their bud-directed ends (Yang and Pon, 2002), but the high density of cables in the bud and neck in a growing yeast cell prevents resolution of the exact filament assembly sites.

To identify the assembly sites of actin cable filaments, we examined yeast with temperature-sensitive actin cables. When yeast with conditional tropomyosin mutations (*tpm1-2 tpm2*Δ) are shifted from 18 to 34.5°C, actin cables disassemble in 1 min, but when restored to 18°C, staining for Tpm1p reveals cable reassembly after 1 min (Pruyne *et al*., 1998). With cable disassembly followed by 1 min of filament reassembly at 18°C, the background of preformed cables is eliminated to reveal only newly assembled filaments at assembly sites. When *tpm1-2/tpm1-2 tpm2*Δ/*tpm2*Δ cells were shifted to 34.5°C for 2 min to disassemble actin cables, and then returned to 18°C for 1 min and stained for Tpm1p distribution, filament assembly was seen at the nascent bud site of unbudded cells, at the bud cortex and neck of small- and medium-budded cells, and at the bud neck/septal plane of large-budded cells (small- and medium-budded cells shown in Figure 4A).

Myo2p provides another probe for actin cable assembly sites. In this assay, Myo2p delocalizes after 2 min of cable disassembly, but it begins to repolarize at cable assembly sites after 1 min at 18°C (Pruyne *et al*., 1998). With filament disassembly and reassembly in these cells, Myo2p began to reappear at the nascent bud site, at small- and medium-sized bud tips, and at the septal plane (small-, medium-, and large-budded cells shown in Figure 4A), indicating the newly formed filaments are functional cables capable of recruiting the myosin. Both sets of results show a correlation between cable assembly sites and formin-rich regions of the cell cortex (the bud cortex and neck).

To examine the persistence of these filament assembly sites, cables were disassembled in *tpm1-2/tpm1-2 tpm2*Δ/*tpm2*Δ cells for varying periods of time at 34.5°C before returning to 18°C for 1 min. After a prolonged absence of actin cables (1 h), cable reassembly and Myo2p recruitment at 18°C occurred at the bud neck rather than the bud cortex (Figure 4A). Looking specifically at Myo2p distribution, we found that the proportion of *tpm1-2/tpm1-2 tpm2*Δ/*tpm2*Δ cells that were able to recruit the myosin to the bud cortex decreased to near zero after 30 min at 34.5°C, whereas the proportion that recruited Myo2p to the neck increased over the same period (Figure 4B), indicating that the ability to assemble cables at the neck persisted through this time, but the ability to assemble cables at the bud cortex (which are required to transport Myo2p to the bud tip) was lost under these conditions.

However, this was not a permanent reorientation of the actin cytoskeleton to the neck for many cells. When *tpm1-2/tpm1-2 tpm2*Δ/*tpm2*Δ cells were shifted to 34.5°C for 1 h, and then restored to 18°C for 20 min, Myo2p returned to the bud tip in the majority of small-budded cells (78%, compared with 95% with tip-associated Myo2p before loss of cables),

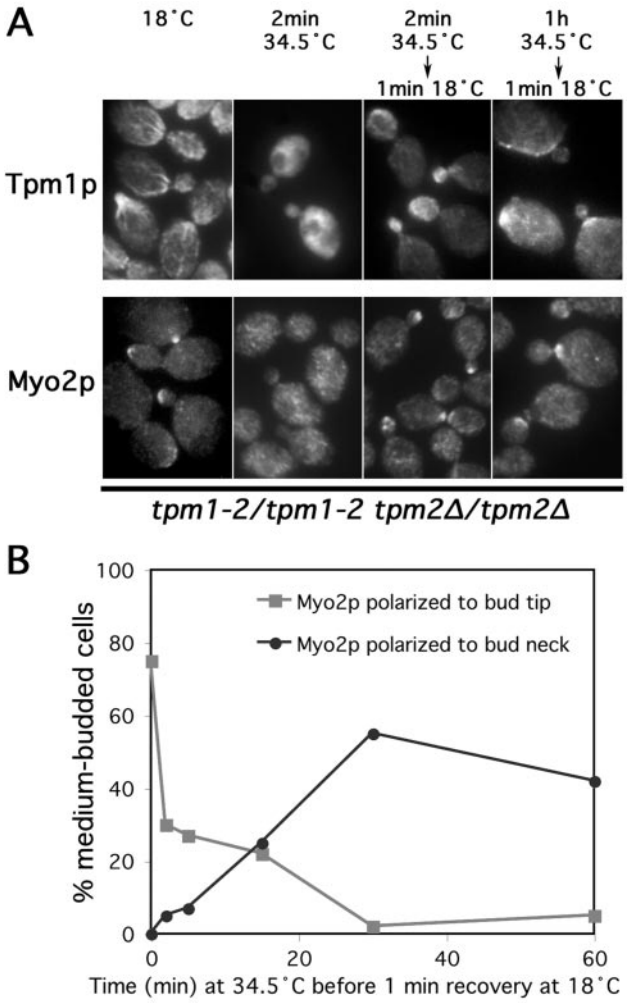

Figure 4. Actin cable filaments assemble at the bud cortex and neck. (A) *Tpm1-2/tpm1-2 tpm2*Δ*/tpm2*Δ mutants (ABY971) were subjected to the indicated conditions and stained to show Tpm1p and Myo2p distributions. (B) *Tpm1-2/tpm1-2 tpm2*Δ*/tpm2*Δ cells (ABY971) were shifted to 34.5°C for varying lengths of time before restoration to 18°C for 1 min and treatment for anti-Myo2p immunofluorescence microscopy. One hundred medium-budded cells from each time point were scored for the presence of Myo2p at the bud tip (gray squares) or neck (black circles).

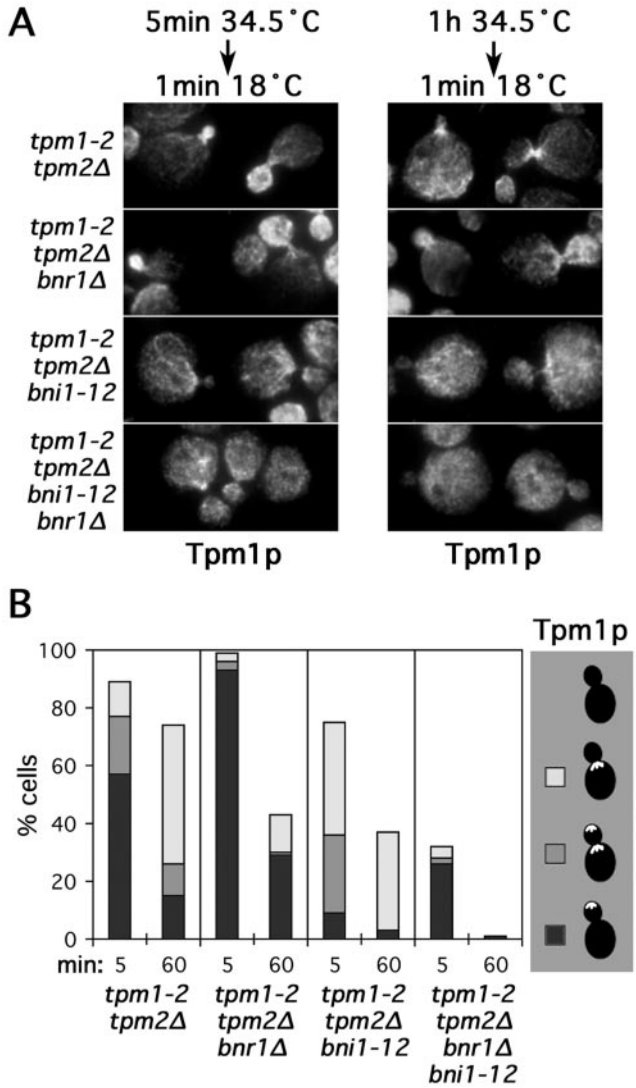

Figure 5. Bni1p and Bnr1p differentially direct bud cortex- and bud neck-associated filament assembly. (A) Strains bearing *tpm1-2 tpm2*Δ (ABY944), *tpm1-2 tpm2*Δ *bnr1*Δ (ABY1804), *tpm1-2 tpm2*Δ *bni1-12* (ABY1805), and *tpm1-2 tpm2*Δ *bni1-12 bnr1*Δ (ABY1806) mutations were subjected to the indicated conditions and stained to show Tpm1p distribution. (B) One hundred medium-budded cells of each strain in A were shifted to 34.5°C for the indicated times before restoration to 18°C for 1 min and staining to show Tpm1p distribution. Cells were scored for the presence of Tpm1p in the bud (black), in the bud and at the neck (gray), at the neck (white), or delocalized (blank). Results for small-budded cells were similar.

whereas tip-directed polarity was regained in a smaller proportion of medium-budded cells (23%, compared with 62% before with tip-associated Myo2p before loss of cables). Thus, the neck-associated cable assembly site is persistent, whereas the cortex-associated cable assembly site is not under these conditions.

To determine whether bud cortex- and neck-associated filament assembly correlated with the activity of the appropriate formin, we examined cable assembly in *tpm1-2 tpm2*Δ yeast bearing *bnr1*Δ and/or an irreversible temperature-sensitive mutation of *BNI1* (*bni1-12*) (Evangelista *et al*., 2002). These strains were subjected to short (5-min) or long (60-min) shifts to 34.5°C before returning to 18°C for 1 min (Figure 5, A and B). In *tpm1-2 tpm2*Δ *bnr1*Δ cells after the short shift, filament reassembly generally occurred at the bud cortex and not at the bud neck, and after the long shift, assembly was either disorganized or occurred at the bud cortex and not the neck (Figure 5B, black bars), in contrast to *tpm1-2 tpm2*Δ controls, where assembly was primarily at the neck (Figure 5B, white bars), showing the absence of Bnr1p diminishes neck-associated filament assembly. The remaining neck-associated assembly suggests that in some cells, Bni1p is present at this location, despite our inability to detect it. For the *tpm1-2 tpm2*Δ *bni1-12* cells, filament assembly at the bud cortex was reduced compared with control *tpm1-2 tpm2*Δ cells after short and long shifts (Figure 5B, black + gray bars), indicating the importance of Bni1p for bud cortex-associated filament assembly, although again a small amount of residual activity at the bud cortex suggests an undetectable amount of Bnr1p is present at that location.

Finally, *tpm1-2 tpm2*Δ *bni1-12 bnr1*Δ cells were nearly unable to assemble cables from the neck under any condition (Figure 5B, absence of gray + white bars), and after the long shift (when *bni1-12* was completely inactivated), were unable to assemble cables at all, consistent with the formin dependence of cable assembly. This correlation between the respective formins and distinct sites of filament assembly suggests the presence of formins at these sites stimulates actin cable assembly there and provides an explanation for the dependence of subsets of actin cables on the two formin isoforms.

Actin Assembly at the Bud Neck Requires the Septins

The persistence of cable assembly activity at the bud neck suggests it associates with a stable landmark. A ring of proteins called septins, encoded by the genes *CDC3*, *CDC10*, *CDC11*, *CDC12*, and *SHS1*, is a prominent landmark of the neck. Septins are recruited to the nascent bud site in a Cdc42p-dependent manner, and then remain at that location as a ring around the neck of the emerging and growing bud, and finally divide into two rings at cell separation (Figure S2A and B; for review, see Field and Kellogg, 1999; Gladfelter *et al*., 2001; Faty *et al*., 2002; Longtine and Bi, 2003). However, the septins play a variety of roles, promoting the proper activation of the B-cyclins for cell cycle progression (Barral *et al*., 1999; McMillan *et al*., 1999; Shulewitz *et al*., 1999; Longtine *et al*., 2000; Hanrahan and Snyder, 2003), maintaining a diffusion barrier between the bud and mother cortices (Barral *et al*., 2000), and recruiting cytokinetic (Bi *et al*., 1998; Lippincott and Li, 1998) and cell wall-synthesizing machinery (DeMarini *et al*., 1997) to the bud neck. To determine whether septins influence actin cable organization, we examined Tpm1p distribution in yeast with a temperature-sensitive *CDC10* septin (*cdc10-1*) (Hartwell, 1971).

When *cdc10-1/cdc10-1* cells were shifted to 35°C for 1 h, the septin scaffold at the bud neck disassembled completely as judged by the absence of a NH_2-terminally GFP-tagged Cdc12p septin from the neck, with GFPCdc12p being largely delocalized or showing a very faint enrichment at cell tips (Figure S3, white arrows). Under these conditions, the *cdc10-1/cdc10-1* cells displayed prominent cables at the tip and along the sides of the bud, but rarely at the bud neck or in the mother (Figure 6A), similar to *bnr1*Δ cells. With 4-h incubation at 35°C, *cdc10-1* cells grew in a highly polarized manner, consistent with the dispensability of neck-associated cables for polarized growth as long as bud-associated actin cables are present.

To determine whether filament assembly at the neck, rather than simply cable anchorage, is dependent on septins, we examined where cable assembly occurred in tropomyosin mutant yeast bearing either of two temperature-sensitive septin mutations (*tpm1-2 tpm2*Δ *cdc10-1* and *tpm1-2 tpm2*Δ *cdc12-6*). Cables were disassembled in these cells and *tpm1-2 tpm2*Δ control cells for short (2-min) or long (60-min) periods at 34.5°C before 1 min recovery at 18°C. After short periods of disassembly, cable reassembly was detected at the bud cortex of all strains, but after long periods of disassembly, the *tpm1-2 tpm2*Δ controls but not the *tpm1-2 tpm2*Δ *cdc10-1* and *tpm1-2 tpm2*Δ *cdc12-6* strains assembled cables at the neck (Figure 6, B and C). Rather, the septin mutations resulted in the sparse assembly of filaments in a disorganized manner, showing that the septins are important for localizing actin cable assembly activity to the bud neck.

A conditional *cdc12-6* mutation has been reported to have only a partial effect on the localization of an overexpressed Bnr1p-derived construct (Kikyo *et al*., 1999), with only ~50% of *cdc12-6* cells losing polarization of the protein after 6 h under restrictive conditions. However, the Bnr1p-derived construct was expressed from the strong *GAL1-10* promoter. To determine whether Bnr1p expressed at the endogenous level depends on the septins for localization, we examined Bnr1pGFP in *cdc10-1/cdc10-1* cells. Compared with wild-type controls, Bnr1pGFP in *cdc10-1/cdc10-1* cells lost nearly all localization after 1 h at 35°C (Figure 6, D and E), demonstrating a strong dependence of Bnr1p on septins for its proper localization.

This loss of neck-associated Bnr1p and cables may explain the synthetic lethality observed between the *cdc12-6* septin mutation and deletion of *BNI1* (which led to the gene name *B*ud *N*eck *I*nteracting 1) (Longtine *et al*., 1996) and between the *cdc10-1* septin mutation and deletion of *SPA2* (Flescher *et al*., 1993), which encodes a Bni1p-binding protein. Specifically, combinations in defects in septin and Bni1p function would be expected to eliminate all cable organization. To address this, we examined yeast harboring the *cdc10-1* mutation and a conditional *bni1-11* mutation (Evangelista *et al*., 2002). Alone, *bni1-11* caused loss of Tpm1p-staining cables from the bud at 35°C, and after prolonged growth, resulted in cells with a variety of morphological defects, varying from highly depolarized cells to those with round buds and a wide neck typical of *bni1*Δ yeast (Figure 6A). In *bni1-11/bni1-11 cdc10-1/cdc10-1* cells, cables were no longer present in the bud or mother after 1 h at 35°C, just as with *bni1-11/bni1-11 bnr1*Δ*/bnr1*Δ or *tpm1-2/tpm1-2 tpm2*Δ*/tpm2*Δ strains (Figure 6A). Prolonged growth of *bni1-11 cdc10-1* cells at 35°C showed uniformly severe polarized growth defects greater than those caused by *bni1-11* or *cdc10-1* alone. The *bni1-11 cdc10-1* cells enlarged to rounded cells that were unable to form buds, similar to *bni1-11 bnr1*Δ and *tpm1-2 tpm2*Δ yeast that completely lack actin cables (Figure 6A). However, the *bni1-11 cdc10-1* cells retained some polarity in that they were each able to form a blunted projection, indicating the cells retained some Bnr1p-dependent polarity, possibly reflecting a partial septin independence of Bnr1p localization in unbudded cells (Figure 6E), or the small amount of cell tip-associated GFP-Cdc12p septin in *cdc10-1/cdc10-1* yeast at 35°C (Figure S3).

Polarized Secretion Maintains Cable Assembly Activity at the Bud Cortex

The loss of cable assembly activity from the buds of *tpm1-2 tpm2*Δ cells after 1 h at 34.5°C suggests some instability in that activity under those conditions. Two possibilities presented themselves. The first possibility was that the retention of actin cable assembly activity within the bud specifically depends on the presence of actin cables. Alternatively, the loss might reflect a nonspecific instability in the association of cable assembly activity with the bud cortex at 34.5°C, whether or not cables are present. Thus, loss of the activity from the bud cortex might be due to trivial factors such as progression through the cell cycle or a limited half-life of components directing cable assembly at the bud cortex.

To resolve whether cable assembly at the bud cortex is inherently unstable at 34.5°C even in the presence of actin cables, we examined yeast that normally undergo prolonged periods of polarized growth to determine whether they maintain bud cortex-associated actin cables for prolonged periods. Yeast polarity is regulated by the cell cycle. The appearance of G1-cyclins trigger initiation of bud growth, whereas B-cyclin activity in the cytoplasm specifically promotes the switch from tip-directed (apical) bud growth to isotropic bud growth (reviewed in Lew and Reed, 1995; Rua *et al*., 2001). Overproduction of G1-cyclins allows for bud initiation, but then it prolongs tip-directed growth, the latter

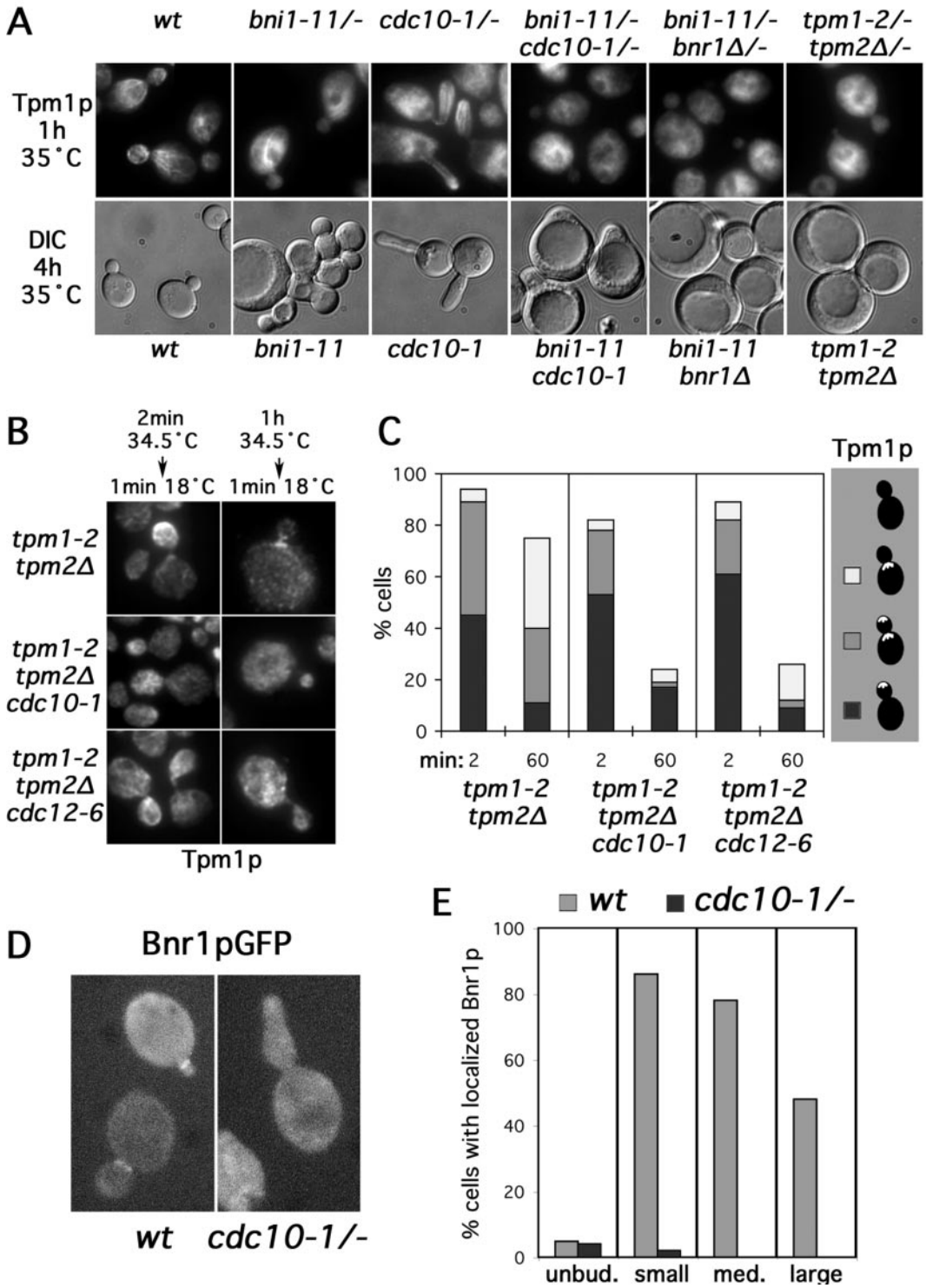

Figure 6. Septins localize Bnr1p-dependent cable assembly to the bud neck. (A) Diploid wild-type (ABY1848), *bni1-11/bni1-11* (ABY2247), *cdc10-1/cdc10-1* (ABY1662), *bni1-11/bni1-11 cdc10-1/cdc10-1* (ABY2248), *bni1-11/bni1-11 bnr1*Δ*/bnr1*Δ (ABY1803), and *tpm1-2/tpm1-2 tpm2*Δ*/tpm2*Δ (ABY2250) were shifted to 35°C for 1 h and stained to show Tpm1p distribution. Corresponding haploid strains (Y1239, ABY2209, ABY2201, ABY2226, ABY2218, and ABY1807) were shifted to 35°C for 4 h and observed by differential interference contrast microscopy. (B) *Tpm1-2 tpm2*Δ (ABY944), *tpm1-2 tpm2*Δ *cdc10-1* (ABY1639), and *tpm1-2 tpm2*Δ *cdc12-6* (ABY1643) cells were subjected to indicated conditions and stained for Tpm1p distribution. (C) Cells of each strain in B were shifted to 34.5°C for the indicated times before 1 min restoration to 18°C and staining to show Tpm1p distribution. One hundred medium-budded cells were scored for the presence of Tpm1p in the bud (black), in the bud and at the neck (gray), at the neck (white), or delocalized (blank). Results for small-budded cells were similar. (D) Bnr1pGFP-fluorescence is shown for wild-type (YEF2255) and *cdc10-1/cdc10-1* mutant cells (ABY2262) after 1 h at 34.5°C. (E) Fifty cells each of unbudded (unbud.) and small- (small), medium- (med.), and large-budded (large) cells treated as in D were assayed for the localization of Bnr1pGFP to a single point on the cell cortex (for unbudded cells) or the bud neck (for budded cells).

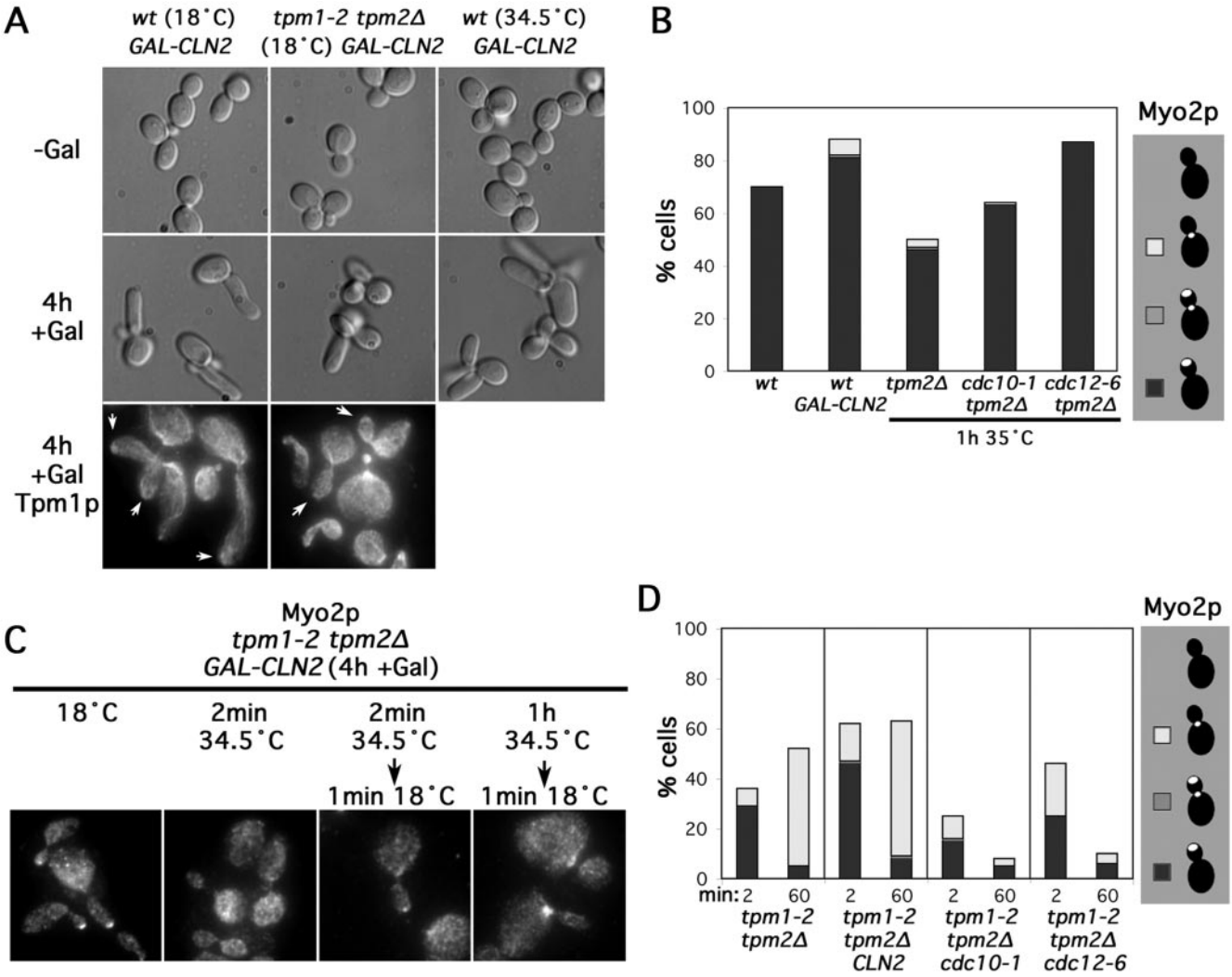

Figure 7. Inhibition of the switch from apical to isotropic bud growth does not preserve bud cortex-associated cable assembly in the absence of actin cables. (A) *GAL-CLN2*–bearing wild-type (ABY2251) and *tpm1-2 tpm2*Δ (ABY 2252) cells either were (+Gal) or were not (−Gal) induced to overproduce Cln2p for 4 h at the indicated temperatures and observed by differential interference contrast microscopy or stained to show Tpm1p distribution. Arrows indicate bud tips with associated Tpm1p. (B) Wild-type (Y1239) or *GAL-CLN2*-bearing (ABY2251) cells induced for 4 h were grown at 18°C and stained for Myo2p. *Tpm2*Δ (ABY945), *cdc10-1 tpm2*Δ (ABY1637), and *cdc12-6 tpm2*Δ (AY1639) cells were grown at 35°C for 1 h before staining to show Myo2p distribution. One hundred cells of each strain with medium-sized and/or elongated buds were scored for the presence of Myo2p at the bud tip (black), at the bud tip and the neck (gray), at the bud neck (white), or not localized (blank). (C) *Tpm1-2 tpm2*Δ *GAL-CLN2* cells (ABY2252) were subjected to the indicated conditions and stained to show Myo2p distribution. (D) *Tpm1-2 tpm2*Δ (ABY944) cells, *tpm1-2 tpm2*Δ *GAL-CLN2* (ABY2252) cells grown 4 h in galactose, *tpm1-2 tpm2*Δ *cdc10-1* (ABY1639) cells, and *tpm1-2 tpm2*Δ *cdc12-6* (ABY1643) cells were shifted to 34.5°C for 2 or 60 min before restoration to 18°C for 1 min and Myo2p localized by immunofluorescence microscopy. One hundred medium-budded cells of each were scored for the presence of Myo2p at the bud tip (black), at the bud tip and neck (gray), at the bud neck (white), or not localized (blank).

likely by indirect inhibition of B-cyclin activity (Lew and Reed, 1993; Ahn *et al*., 2001).

We introduced into wild-type yeast an inducible G1-cyclin–encoding *CLN2* (*GAL-CLN2*) and induced Cln2p production for 4 h at either 18 or 34.5°C. At both temperatures, we found cells exhibited elongated buds, indicative of prolonged apical growth (Figure 7A). Tpm1p staining showed cables were associated with the bud tip and the cortex of these elongated buds as well as with the bud necks and in the mother cells, and Myo2p staining was concentrated at their bud tips (Figure 7, A and B). Thus, Cln2p-overproduction was able to prolong the time during which cable assembly occurred at the bud tip. Similar results were obtained with yeast bearing either conditional septin mutation *cdc10-1* or *cdc12-6*, both of which also result in inhibition of B-cyclin activity (for a mechanistic explanation, see Moffat and Andrews, 2003), and which induced elongated buds after 1 h at 35°C with bud cortex-associated actin cables and Myo2p (Figures 6A and 7B). Thus, appropriate cell cycle manipulations suggest that the association of cable assembly activity with the bud cortex is not inherently unstable at elevated temperatures.

To determine whether these cell cycle perturbations would be sufficient to preserve cable assembly activity at the bud cortex in the absence of actin cables, we examined the effects of Cln2p-overproduction in *tpm1-2 tpm2*Δ cells. At 18°C, Gal-induction of *tpm1-2 tpm2*Δ *GAL-CLN2* cells promoted tip-directed growth and bud cortex-associated cables

and Myo2p just as for wild-type cells (Figure 7, A and C). When shifted to 34.5°C, cables disassembled and Myo2p delocalized in the *tpm1-2 tpm2*Δ *GAL-CLN2* cells, just as for *tpm1-2 tpm2*Δ cells (Figure 7C). When the *tpm1-2 tpm2*Δ *GAL-CLN2* were then restored to 18°C for 1 min and stained for Myo2p, we found the results were nearly identical to those of the *tpm1-2 tpm2*Δ controls: after brief cable disassembly and reassembly, Myo2p was recruited along cables to the bud tip, but after prolonged actin cable disassembly followed by reassembly, Myo2p was recruited along cables to the bud neck with the same efficiency as for *tpm1-2 tpm2*Δ cells not overproducing Cln2p (Figure 7, C and D). Thus, Cln2p-overproduction had no impact on the ability of yeast to maintain actin cable assembly activity at the bud cortex in the absence of actin cables.

Similar results were seen when the septin mutations *cdc10-1* and *cdc12-6* were introduced into *tpm1-2 tpm2*Δ yeast. With prolonged incubation at 35°C, the ability to assemble actin cables on the bud cortex or recruit Myo2p to the bud tip upon restoration to 18°C was lost in *tpm1-2 tpm2*Δ *cdc10-1* and *tpm1-2 tpm2*Δ *cdc12-6*, despite the expectation that passage through the cell cycle is inhibited (Figures 6, B and C, and 7D).

In *tpm1-2 tpm2*Δ cells without cell cycle perturbations, we also found evidence that loss of tip-directed polarity in the absence of cables was not dependent on passage through the cell cycle. Specifically, as mentioned previously, the majority of small-budded *tpm1-2/tpm1-2 tpm2*Δ*/tpm2*Δ were able to regain tip-associated Myo2p when allowed to recover for 20 min at 18°C after lacking actin cables for 1 h. Similarly, when haploid *tpm1-2 tpm2*Δ yeast were shifted to 34.5°C for 1 h, and then restored to 18°C for 15 min, Myo2p became associated with the bud cortex of 68% small-budded cells (compared with 96% before the loss of actin cables) and 35% medium-budded cells (compared with 60% before the loss of actin cables). The short period of recovery and the high proportion of small-budded cells with tip-associated Myo2p argue against these solely representing new buds that have formed, and their appearance is inconsistent with passage of these cells through the cell cycle to the point where the cytoskeleton reorients toward the neck for cell division. Rather, these results indicate that the ability to assemble actin cables at the bud cortex was lost specifically due to the absence of actin cables, not cell cycle progression.

One explanation for the dependence of bud cortex-associated cable assembly activity on the presence of actin cables is that the cables might directly anchor such a component. However, the loss of bud cortex-associated assembly activity was gradual (Figure 4B), suggesting an indirect dependence on actin cables. An alternative explanation for this cable dependence is that some factor important to cable assembly is gradually lost from the bud cortex but continually replenished by transport along the cables.

If Myo2p were important in transporting such a factor, we would expect defects in Myo2p to result in the loss of bud cortex-associated actin cables and Myo2p. We examined yeast bearing a temperature-sensitive mutation of the Myo2p COOH-terminal domain (*myo2-16*). At 35°C, this mutant Myo2p still polarizes in response to actin cables, but it is unable to deliver secretory vesicles (Schott *et al*., 1999). At 18°C, actin cables and Myo2p distribution in *myo2-16/myo2-16* seemed normal, but after 1 h at 35°C, cables were largely absent from the bud, and the mutant Myo2p, when polarized, was found at the bud neck (Figure 8, A–C). Such a shift was not seen in wild-type yeast, suggesting maintenance of actin cable assembly activity at the bud cortex depends on Myo2p. The loss of tip-directed polarity in these cells occurred over a very similar time course as in *tpm1-2 tpm2*Δ yeast (compare Figures 4B and S4), consistent with a common mechanism.

To determine whether secretory vesicles might carry a putative cable-assembly factor, we investigated whether blocks in secretion cause a loss of cables or Myo2p from the bud. Among proteins critical for the fusion of secretory vesicles with the plasma membrane are the rab-GTPase Sec4p (Salminen and Novick, 1987), its guanine-nucleotide-exchange-factor Sec2p (Walch-Solimena *et al*., 1997), and a protein complex termed the exocyst (composed of Sec3p, 5p, 6p, 8p, 10p, 15p, Exo70p, and Exo84p) (TerBush and Novick, 1995; TerBush *et al*., 1996; Guo *et al*., 1999). Temperature-sensitive mutations of these result in accumulation of post-Golgi secretory vesicles and an exocytic block at restrictive temperatures (Novick *et al*., 1980, 1981; Guo *et al*., 1999). When a collection of such mutants (*sec2-41/sec2-41*, *sec4-8/sec4-8*, *sec6-4/sec6-4*, *sec10-2/sec10-2*, *sec15-1/sec15-1*) was grown at 18°C, Myo2p and Tpm1p distribution seemed normal, but after 1 h at 35°C, all showed a decreased proportion of cells with cables and Myo2p associated with the bud cortex and an increased proportion with Myo2p concentrated at the bud neck (Figure 8, A–C).

As with defects in actin cables or Myo2p function, the shift in actin-based polarity to the neck in these cells occurred gradually over the course of 1 h (Figure S4). This is consistent with a requirement for secretion to maintain cable assembly activity at the bud cortex. However, this interpretation is complicated in that for many of these *sec* mutants, the overall localization of Myo2p was very poor, yet Myo2p itself is required to maintain cable assembly activity at the bud cortex. Thus, it was possible that in these mutants, the loss of bud cortex-associated cables was an indirect effect of delocalizing Myo2p.

We hypothesized that the association of Myo2p with the accumulated post-Golgi vesicles in some late *sec* mutants (Wagner *et al*., 2002) might interfere with the localization of the myosin in these cells. To avoid this, we also examined cable and Myo2p distribution in yeast bearing conditional blocks in earlier steps of the secretory pathway. Temperature-sensitive mutations affecting a COPII component (*sec23-1*) (Barlowe *et al*., 1994) or a protein involved in packaging COPII-coated vesicles (*sec16-2*) (Campbell and Schekman, 1997) result in the accumulation of secretory products in the endoplasmic reticulum at the restrictive temperature (Novick *et al*., 1980, 1981). When such cells were shifted to 35°C for 1 h, both showed a depletion of actin cables from the bud and increased association of Myo2p with the bud neck (Figure 8, A–C). Unlike in some of the late *sec* mutants, Myo2p in these cells was polarized in a similar proportion of cells as a wild-type control, suggesting the altered cable distribution was not caused by direct interference of Myo2p function. Thus, depolarization or blockage of secretion reduces the presence of bud cortex-associated cables, consistent with the dependence of some cable assembly factor on the secretory pathway for delivery to the bud cortex.

Rho-GTPases Depend on Polarized Secretion for Bud Tip-Association

To determine whether any factors known to be important for cable assembly depend on actin cables for their localization, we examined the distribution of a variety of such proteins in wild-type and *tpm1-2/tpm1-2 tpm2*Δ*/tpm2*Δ yeast at 34.5°C. Serving as controls, Bnr1pGFP and GFPCdc12p largely remained associated with the bud neck of small- and medium-budded *tpm1-2/tpm1-2 tpm2*Δ*/tpm2*Δ cells, as judged by anti-GFP immunofluorescence (Figure 9, A and B), consistent

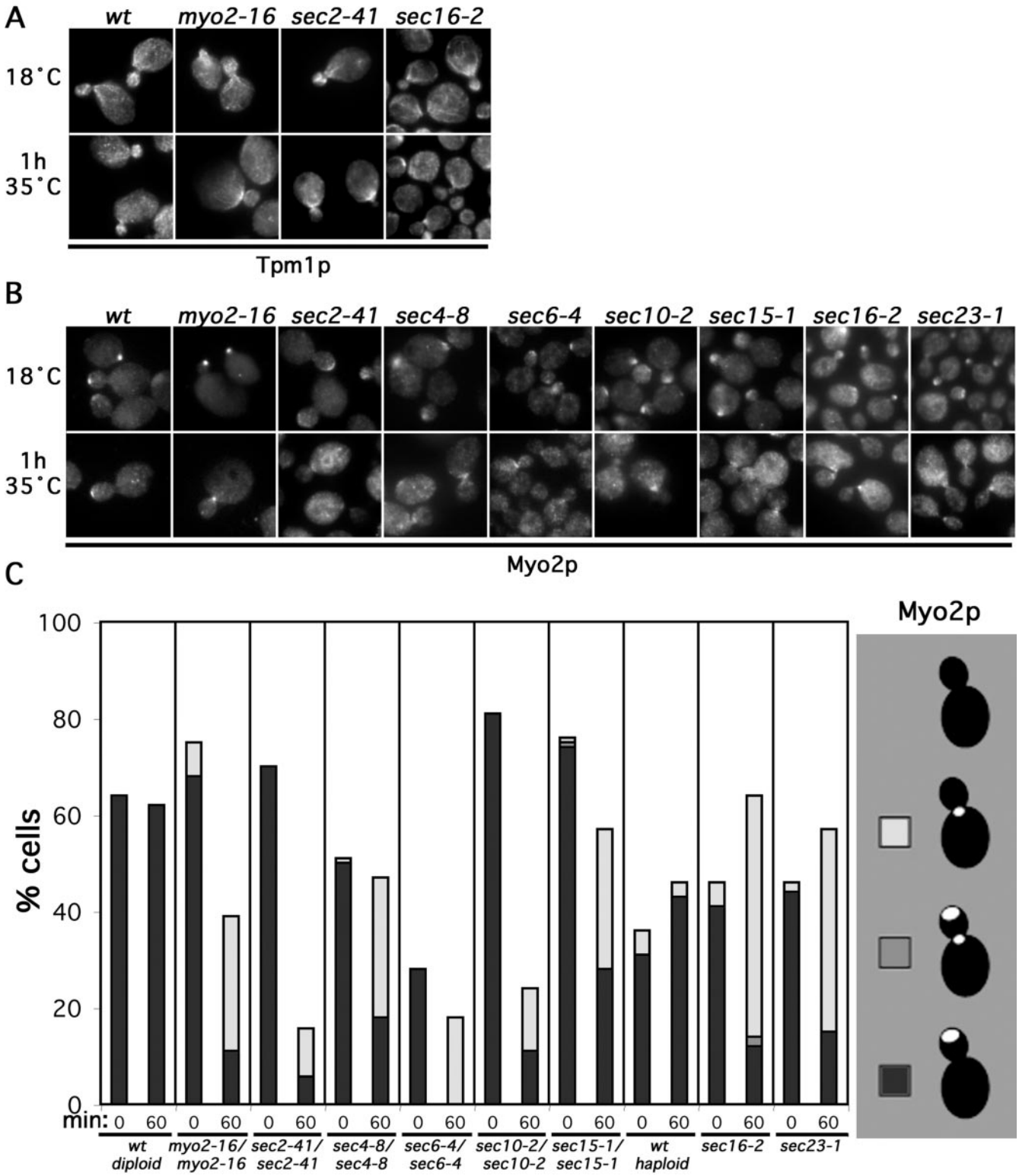

Figure 8. Disruption of polarized secretion depletes bud-associated cables. (A) Wild-type (ABY501), *myo2-16/myo2-16* (ABY506), *sec2-41/sec2-41* (ABY1665), and *sec16-2* (RSY267) cells were subjected to the indicated conditions and stained to show Tpm1p distribution. (B) Wild-type (ABY501), *myo2-16/myo2-16* (ABY506), *sec2-41/sec2-41* (ABY1665), *sec4-8/sec4-8* (ABY994), *sec6-4/sec6-4* (ABY993), *sec10-2/sec10-2* (ABY995), *sec15-1/sec15-1* (ABY996), *sec16-2* (RSY267), and *sec23-1* (RSY281) cells were subjected to the indicated conditions and stained to show Myo2p distribution. (C) One hundred medium-budded cells of each sample in B plus the wild-type haploid RSY255 were scored for the presence of Myo2p at the bud tip (black), the bud tip and neck (gray), the neck (white), or delocalized (blank). Results were similar for small-budded cells.

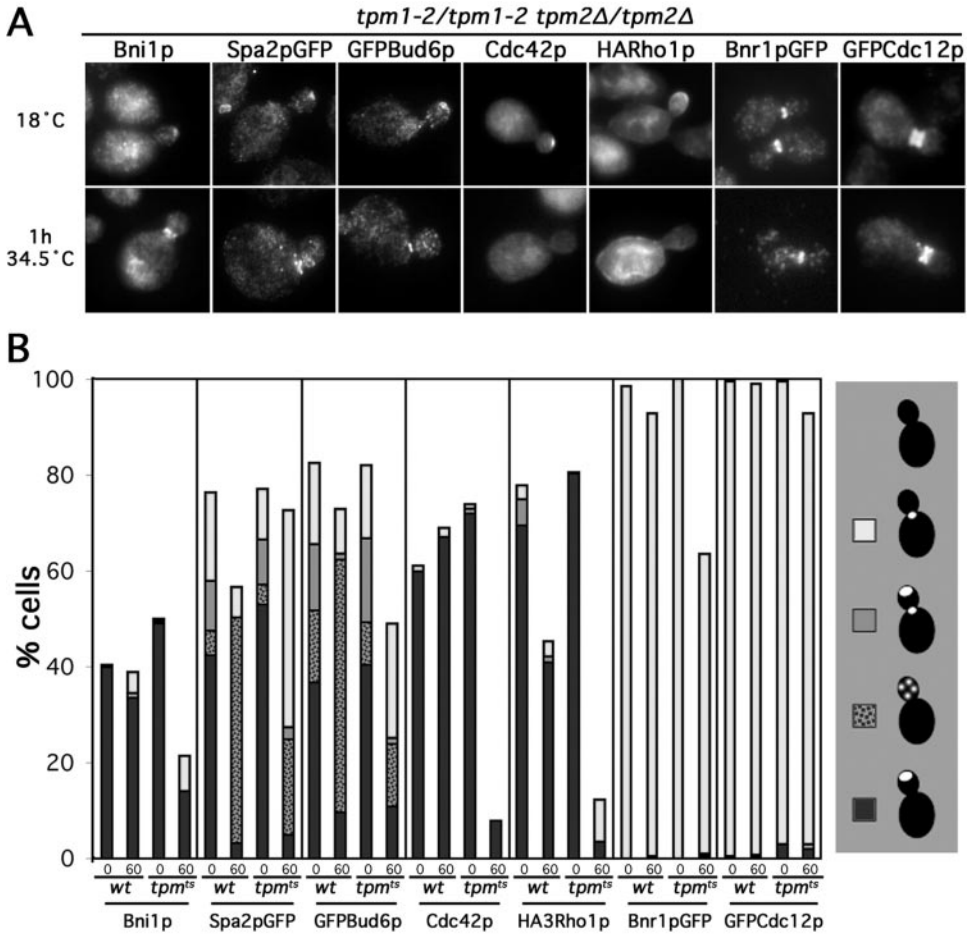

Figure 9. Rho-proteins, but not other cable-assembly factors, strongly depend on cables for retention at the bud tip. (A) *Tpm1-2/tpm1-2 tpm2*Δ*/tpm2*Δ strains expressing Spa2pGFP (ABY1197), GFPBud6p (ABY1171), HARho1p (ABY1602), Bnr1pGFP (ABY1891), GFPCdc12p (ABY1899), or no epitope-tagged protein (ABY971) were subjected to the indicated growth conditions and stained to show Bni1p, GFP, Cdc42p, and HA-epitope distributions. Examples of aberrant Bni1p, Spa2pGFP, GFPBud6p, Cdc42p, and HARho1p localization at 34.5°C are shown. (B) Small- and medium-budded cells of each sample in A plus identically treated *TPM1/TPM1 tpm2*Δ*/tpm2*Δ control strains expressing Spa2pGFP (ABY1198), GFPBud6p (ABY1199), HARho1p (ABY1601), GFPCdc12p (ABY1896), or no epitope-tagged protein (ABY973), or *TPM1/TPM1 TPM2/TPM2* Bnr1pGFP control strain (YEF2255), were scored for the presence of stain at the bud tip (black), as puncta along the bud cortex (speckled), at the bud tip and neck (gray), at the neck (white), or delocalized (blank). For strains ABY1171, 1197, 1198, 1199, 1601, and 1602, 200 small- and 200 medium-budded cells of each were scored and averaged. For the remaining strains, 100 small- and 100 medium-budded cells of each strain were scored and averaged.

with the persistence of the neck-associated cable assembly site. The association of Bni1p with the bud cortex was reduced in *tpm1-2/tpm1-2 tpm2*Δ*/tpm2*Δ cells after 1 h at 34.5°C (Figure 9, A and B). However, a reduction of cortical Bni1p also was seen in the *TPM1/TPM1 tpm2*Δ*/tpm2*Δ controls, and in small-budded cells in particular, the proportion of *tpm1-2/tpm1-2 tpm2*Δ*/tpm2*Δ cells retaining detectable Bni1p at the bud tip (36%) was nearly identical to that of the *TPM1/TPM1 tpm2*Δ*/tpm2*Δ control cells (39%). This suggests that loss of Bni1p localization in the absence of cables is not likely to account for the loss of cable assembly activity from the bud cortex of tropomyosin mutant yeast at 34.5°C. Consistent with this, wild-type yeast expressing Bni1pGFP from a high-copy plasmid did not display any fluorescent particles undergoing directed movements indicative of Myo2p-dependent transport of post-Golgi vesicles.

Bud6p and Spa2p are two components of a Bni1p-binding protein complex called the polarisome (Sheu *et al*., 1998) that localizes to growth sites with Bni1p (Snyder, 1989; Amberg *et al*., 1997). Bud6p cooperates with Bni1p in promoting actin assembly in vivo (Evangelista *et al*., 2002; Sagot *et al*., 2002a) and in vitro (Moseley *et al*., 2004) and associates with secretory vesicles (Jin and Amberg, 2000), and in the absence of Bud6p, cables are very sparse (Amberg *et al*., 1997). Spa2p is required for the proper localization of Bni1p to the bud tip (Fujiwara *et al*., 1998), and in its absence, cables are specifically absent from the bud, similar to *bni1*Δ cells (our unpublished data). Shift of either control or *tpm1-2/tpm1-2 tpm2*Δ*/tpm2*Δ cells resulted in GFPBud6p and Spa2pGFP redistributing from the bud tip to puncta along the bud cortex and to the bud neck (Figure 9, A and B). Roughly half the proportion of *tpm1-2/tpm1-2 tpm2*Δ*/tpm2*Δ cells retained both fusion proteins within the bud compared with control cells, suggesting neither protein represents the critical cable-assembly factor lost under these conditions. As further support, Spa2pGFP in live yeast did not display directed movements of fluorescent particles, suggesting this protein also is not recruited to the bud cortex by targeted secretion.

The rho-GTPases Cdc42p and Rho1p also localize to growth sites (McCaffrey *et al*., 1991; Ziman *et al*., 1993; Yamochi *et al*., 1994) and interact with Bni1p in two-hybrid assays (Kohno *et al*., 1996; Evangelista *et al*., 1997). Cdc42p is required for recruitment of Bni1p to the nascent bud site (Jaquenoud and Peter, 2000; Ozaki-Kuroda *et al*., 2001) and when overexpressed, Cdc42p promotes Bni1p-dependent cable assembly (Dong *et al*., 2003). Rho1p is required for Bni1p- and Bnr1p-dependent cable assembly, at least at 37°C (Tolliday *et al*., 2002; Dong *et al*., 2003). Also, both rho-GTPases associate with secretory vesicles (Abe *et al*., 2003; Wedlich-Soldner *et al*., 2003). For endogenous Cdc42p and NH_2-terminally HA-tagged Rho1p expressed from the *RHO1* locus, actin cable disassembly in *tpm1-2/tpm1-2 tpm2*Δ*/tpm2*Δ cells resulted in delocalization (Figure 9, A and B). After 1 h at 34.5°C, the fraction of tropomyosin mutants retaining Cdc42p at the bud cortex was only 12% that of wild-type controls, and the fraction of mutants retaining HARho1p at the bud cortex was only 8% of that of controls. Thus, these two proteins are strong candidates for cable-

dependent factors important for promoting Bni1p-stimulated filament assembly on the bud cortex.

DISCUSSION

Our results help reconcile the similar biochemical functions of the two formins, Bni1p and Bnr1p, with the distinct phenotypes of their loss of function. Both formins promote actin cable assembly (Evangelista *et al*., 2002; Sagot *et al*., 2002a), but the loss of Bnr1p causes only a mild delay in cell separation (Vallen *et al*., 2000), whereas the absence of Bni1p causes a widened bud neck (Jansen *et al*., 1996; Zahner *et al*., 1996; Mosch and Fink, 1997; Sheu *et al*., 2000), an inability to engage in tip-directed growth (Evangelista *et al*., 1997; Mosch and Fink, 1997; Sheu *et al*., 2000; Ozaki-Kuroda *et al*., 2001), a defect in bipolar bud site selection (Zahner *et al*., 1996), a partial defect in cytokinetic ring contraction (Vallen *et al*., 2000), a defect in early spindle alignment (Fujiwara *et al*., 1999; Lee *et al*., 1999), and a variety of synthetic lethal genetic interactions (Kohno *et al*., 1996; Longtine *et al*., 1996; Fujiwara *et al*., 1998; Fujiwara *et al*., 1999; Lee *et al*., 1999; Tong *et al*., 2001, 2004). We suggest that many, if not all, of these can be attributed to the actin assembly activity of the two formins in conjunction with their specific localizations.

Bnr1p becomes well localized only after bud emergence, associating with the bud neck throughout bud growth. It is required for the strong assembly of tropomyosin-enriched actin filaments at the neck, which gives rise to bundles of actin cables anchored at the neck that permeate the mother cell. These cables behave as a stable mother/bud axis of polarity, because their organization remains unchanged throughout growth of the bud, and this Bnr1p-dependent assembly site remains associated with the bud neck in the face of perturbations such as actin cable disassembly. The localization of Bnr1p depends upon the septins, a group of related proteins that form a scaffold of filaments girding the bud neck. The septin dependence of Bnr1p provides a likely explanation for the synthetic lethality between defects in Bni1p function and septins (Longtine *et al*., 1996), which recapitulate the lethality of the simultaneous loss of Bni1p- and Bnr1p-dependent cable assembly (Figure 5A). Septin-dependent recruitment of Bnr1p also might explain the delay in Bnr1p recruitment to the bud neck until after bud emergence, because during this transition the septins undergo significant changes in their organization (reviewed in Gladfelter *et al*., 2001; recent results in Caviston *et al*., 2003; Dobbelaere *et al*., 2003).

With the absence of Bnr1p-dependent cables, myosin-V–associated membranes are less efficient in initiating directed movements toward the bud, consistent with the reduced presence of actin cables in the mother cell. However, strains lacking Bnr1p still transport vesicles from the mother to concentrate at the bud tip (Figure 3A) and are able to grow with a normal morphology and rate (Imamura *et al*., 1997; Vallen *et al*., 2000), suggesting that the few Bni1p-dependent cables in the mother cell meet the transport requirements of the yeast cell under the conditions examined so far.

In unbudded cells, Bni1p localizes to the nascent bud site before bud emergence to promote assembly of an array of actin cables. This initial recruitment depends on Cdc42p, possibly through bridged interactions between the Cdc42p-effector Gic2p and the Bni1p-binding proteins Spa2p and Bud6p (Jaquenoud and Peter, 2000). The absence of Bni1p disrupts normal cable organization in these cells, resulting instead in formation of a disorganized mesh of Bnr1p-dependent filaments. Presumably, the septins, which are polarized in both wild-type and *bni1*Δ unbudded cells (Figure S2A and B), provide the cue by which Bnr1p is weakly polarized in unbudded cells, because yeast lacking both Bni1p function and septin function are unable to initiate a normal bud (Figure 6A). The guidance of bud emergence by this disorganized mesh of Bnr1p-dependent cables may provide an explanation for the widened neck of *bni1*Δ cells (Jansen *et al*., 1996; Zahner *et al*., 1996; Mosch and Fink, 1997; Sheu *et al*., 2000), a feature that also may indirectly explain the cytokinetic ring contraction defects (Vallen *et al*., 2000), and minor defects seen in the septin ring of *bni1*Δ yeast (Figure S2A, middle *bni1*Δ/*bni1*Δ cell).

In cells with growing buds, Bni1p shows a variable localization on the bud cortex that correlates with an axis of transport toward the changing location of growth sites through the cell cycle (Ozaki-Kuroda *et al*., 2001). Bni1p is required to efficiently assemble cable filaments within the bud, and the absence of Bni1p (by *bni1*Δ) or Bni1p-dependent cables (by disruption of polarized secretion) prevents the directed movements of myosin-associated cargoes from the bud neck to the growing bud tip. As a result, Myo2p and secretory vesicles accumulate at the bud neck or associate with the bud cortex diffusely, rather than concentrating at the bud tip. This provides an explanation for the inability of *bni1*Δ yeast to undergo tip-directed growth (Evangelista *et al*., 1997; Mosch and Fink, 1997; Sheu *et al*., 2000; Ozaki-Kuroda *et al*., 2001) or to bud in a bipolar manner (Zahner *et al*., 1996), which in turn requires tip-directed growth (Sheu *et al*., 2000). Other myosin-V–dependent cargoes also lose their tip-association in *bni1*Δ cells, including the microtubule anchoring protein Kar9p (Miller *et al*., 1999), cytoplasmic microtubules (Segal *et al*., 2000), and the *ASH1* mRNA (Takizawa *et al*., 1997; Beach *et al*., 1999), explaining the inability of *bni1*Δ yeast to orient the mitotic spindle early in the cell cycle (Fujiwara *et al*., 1999; Lee *et al*., 1999) or to properly restrict Ash1p-mediated cell differentiation to daughter cells (Jansen *et al*., 1996).

Based on assays of filament reassembly after short periods of filament disassembly, Bni1p-dependent assembly seems to be more robust than Bnr1p-dependent assembly, with the majority of newly assembled filaments in budded cells occurring along the bud cortex rather than at the bud neck (Figure 4A). But unlike the Bnr1p-dependent axis of polarity, Bni1p-dependent polarity is only meta-stable in that its persistence depends on continued polarized secretion, which in turn depends on transport along actin cables. Thus, when filaments are reassembled after a prolonged period in the absence of actin cables, Bni1p-dependent assembly is reduced compared with Bnr1p-stimulated filament assembly. This loss of Bni1p-dependent cable assembly from the bud cortex occurs in a variety of defects in polarized secretion and does not depend on progression of the cell cycle (Figure 6). However, the loss of Bni1p-dependent cables from the bud occurred only gradually after disruption of polarized secretion, suggesting that some factor is gradually depleted from the bud cortex and continually replenished by association with secretory vesicles transported to the bud cortex along actin cables.

This reduction of Bni1p-dependent assembly does not correlate well with a loss of Bni1p from the bud cortex, nor the Bni1p-binding polarisome proteins Spa2p or Bud6p, despite the fact that Bud6p, at least, is transported on secretory vesicles (Jin and Amberg, 2000). However, two rho-GTPases, Cdc42p and Rho1p, strongly depend on actin cables for their maintenance at the bud cortex, and both have been shown to associate with secretory vesicles (Abe *et al*., 2003; Wedlich-Soldner *et al*., 2003). Because both of these have been implicated in promoting activation of Bni1p (although by unclear

mechanisms; Dong *et al*., 2003), they represent two potential critical factors that are transported along the cables, although other factors are certainly possible. Interestingly, Bni1p, but not Bnr1p, also depends on the rho-GTPase Rho3p for activation (Dong *et al*., 2003). The requirement of Rho3p for efficient fusion of secretory vesicles with the plasma membrane (Adamo *et al*., 1999) may contribute to an explanation for this dependence.

The coupling of formin-activating molecules to secretion provides a potential explanation for why the Bni1p-dependent assembly system depends on the presence of polarized cables, whereas the Bnr1p-dependent system does not. Under normal growth conditions, rho-GTPases or other activators continually cycle through rounds of endocytosis and delivery back to the bud tip by secretion, resulting in enrichment of those factors near Bni1p and the preeminence of Bni1p-dependent filament assembly over Bnr1p-dependent assembly. With depolarization of secretion, the rho-GTPases or other critical factors are endocytosed from the bud and reappear at the mother cortex (Figure 9A). Bnr1p would then gain preeminence either by its continued contact with putative formin-activators now present on the mother cortex, or perhaps by being regulated by factors not subject to membrane traffic at all.

With the restoration of polarized secretion, Bnr1p-dependent cables would initially guide vesicles, resulting in vesicle accumulation at the bud neck and diffusely along the bud cortex (as seen with *bni1*Δ cells). As putative formin-activating factors become enriched in the bud, Bni1p would gradually resume function, restoring transport to the bud tip and reestablishing the tip-directed positive-feedback loop. Future studies may determine whether the dependence of the dynamic Bni1p-driven axis on this positive feedback signal serves as a point of regulation during polarized growth in response to pheromones, cell cycle progression, or stress responses, where realignment or temporary disruption of polarized growth reflects a reduced cable-dependent recruitment of Myo2p and vesicles to the growing cell tip.

Our results indicate budding yeast maintain two axes of polarity by coupling the common core cytoskeletal elements of formin-stimulated filaments to distinct cortical landmarks. One axis provides an entraining signal to direct polarity into the bud, whereas the other allows dynamic targeting of class-V myosins and their cargoes within the bud for proper morphogenesis, with the availability of activating factors providing a key difference between the two. Future studies to elucidate links between the formins, cortical landmarks, and factors important to their activation in yeast may serve as a blueprint for mechanisms used to control the persistence of cytoskeletal polarity in other systems.

ACKNOWLEDGMENTS

We thank D. Amberg, R. Arokowitz, R. Collins, D. Drubin, H. Fares, D. Johnson, K. Kozminski, M. Longtine, P. Novick, J. Pringle, T. Richman, R. Schekman, C. Shamu, and P. Silver for kindly supplying reagents, and J. Ingraffea and B. Judson for providing technical assistance. This work was supported by National Institutes of Health grants GM-39066 (A.B.) and GM-59216 (E.B.).

REFERENCES

Abe, M., Qadota, H., Hirata, A., and Ohya, Y. (2003). Lack of GTP-bound Rho1p in secretory vesicles of Saccharomyces cerevisiae. J. Cell Biol. *162*, 85–97.

Adamo, J.E., Rossi, G., and Brennwald, P. (1999). The Rho GTPase Rho3 has a direct role in exocytosis that is distinct from its role in actin polarity. Mol. Biol. Cell *10*, 4121–4133.

Adams, A.E., and Pringle, J.R. (1984). Relationship of actin and tubulin distribution to bud growth in wild-type and morphogenetic-mutant *Saccharomyces cerevisiae*. J. Cell Biol. *98*, 934–945.

Ahn, S.H., Tobe, B.T., Fitz Gerald, J.N., Anderson, S.L., Acurio, A., and Kron, S.J. (2001). Enhanced cell polarity in mutants of the budding yeast cyclin-dependent kinase Cdc28p. Mol. Biol. Cell *12*, 3589–3600.

Amberg, D.C., Botstein, D., and Beasley, E.M. (1995). Precise gene disruption in *Saccharomyces cerevisiae* by double fusion polymerase chain reaction. Yeast *11*, 1275–1280.

Amberg, D.C., Zahner, J.E., Mulholland, J.W., Pringle, J.R., and Botstein, D. (1997). Aip3p/Bud6p, a yeast actin-interacting protein that is involved in morphogenesis and the selection of bipolar budding sites. Mol. Biol. Cell *8*, 729–753.

Arkowitz, R.A., and Lowe, N. (1997). A small conserved domain in the yeast Spa2p is necessary and sufficient for its polarized localization. J. Cell Biol. *138*, 17–36.

Barlowe, C., Orci, L., Yeung, T., Hosobuchi, M., Hamamoto, S., Salama, N., Rexach, M.F., Ravazzola, M., Amherdt, M., and Schekman, R. (1994). COPII: a membrane coat formed by Sec proteins that drive vesicle budding from the endoplasmic reticulum. Cell *77*, 895–907.

Barral, Y., Mermall, V., Mooseker, M.S., and Snyder, M. (2000). Compartmentalization of the cell cortex by septins is required for maintenance of cell polarity in yeast. Mol. Cell *5*, 841–851.

Barral, Y., Parra, M., Bidlingmaier, S., and Snyder, M. (1999). Nim1-related kinases coordinate cell cycle progression with the organization of the peripheral cytoskeleton in yeast. Genes Dev. *13*, 176–187.

Beach, D.L., Salmon, E.D., and Bloom, K. (1999). Localization and anchoring of mRNA in budding yeast. Curr. Biol. *9*, 569–578.

Bi, E., Maddox, P., Lew, D.J., Salmon, E.D., McMillan, J.N., Yeh, E., and Pringle, J.R. (1998). Involvement of an actomyosin contractile ring in Saccharomyces cerevisiae cytokinesis. J. Cell Biol. *142*, 1301–1312.

Bi, E., and Pringle, J.R. (1996). ZDS1 and ZDS2, genes whose products may regulate Cdc42p in *Saccharomyces cerevisiae*. Mol. Cell. Biol. *16*, 5264–5275.

Bretscher, A. (2003). Polarized growth and organelle segregation in yeast: the tracks, motors, and receptors. J. Cell Biol. *160*, 811–816.

Caviston, J.P., Longtine, M., Pringle, J.R., and Bi, E. (2003). The role of Cdc42p GTPase-activating proteins in assembly of the septin ring in yeast. Mol. Biol. Cell *14*, 4051–4066.

Campbell, J.L., and Schekman, R. (1997). Selective packaging of cargo molecules into endoplasmic reticulum-derived COPII vesicles. Proc. Natl. Acad. Sci. USA *94*, 837–842.

Chang, F., and Peter, M. (2003). Yeasts make their mark. Nat. Cell Biol. *5*, 294–299.

DeMarini, D.J., Adams, A.E., Fares, H., De Virgilio, C., Valle, G., Chuang, J.S., and Pringle, J.R. (1997). A septin-based hierarchy of proteins required for localized deposition of chitin in the *Saccharomyces cerevisiae* cell wall. J. Cell Biol. *139*, 75–93.

Dobbelaere, J., Gentry, M.S., Hallberg, R.L., and Barral, Y. (2003). Phosphorylation-dependent regulation of septin dynamics during the cell cycle. Dev. Cell *4*, 345–357.

Dong, Y., Pruyne, D., and Bretscher, A. (2003). Formin-dependent actin assembly is regulated by distinct modes of Rho signaling in yeast. J. Cell Biol. *161*, 1081–1092.

Evangelista, M., Blundell, K., Longtine, M.S., Chow, C.J., Adames, N., Pringle, J.R., Peter, M., and Boone, C. (1997). Bni1p, a yeast formin linking cdc42p and the actin cytoskeleton during polarized morphogenesis. Science *276*, 118–122.

Evangelista, M., Pruyne, D., Amberg, D.C., Boone, C., and Bretscher, A. (2002). Formins direct Arp2/3-independent actin filament assembly to polarize cell growth in yeast. Nat. Cell Biol. *4*, 260–269.

Evangelista, M., Zigmond, S., and Boone, C. (2003). Formins: signaling effectors for assembly and polarization of actin filaments. J. Cell Sci. *116*, 2603–2611.

Faty, M., Fink, M., and Barral, Y. (2002). Septins: a ring to part mother and daughter. Curr. Genet *41*, 123–131.

Field, C.M., and Kellogg, D. (1999). Septins: cytoskeletal polymers or signalling GTPases? Trends Cell Biol. *9*, 387–394.

Flescher, E.G., Madden, K., and Snyder, M. (1993). Components required for cytokinesis are important for bud site selection in yeast. J. Cell Biol. *122*, 373–386.

Fujiwara, T., Tanaka, K., Inoue, E., Kikyo, M., and Takai, Y. (1999). Bni1p regulates microtubule-dependent nuclear migration through the actin cytoskeleton in Saccharomyces cerevisiae. Mol. Cell. Biol. *19*, 8016–8027.

Fujiwara, T., Tanaka, K., Mino, A., Kikyo, M., Takahashi, K., Shimizu, K., and Takai, Y. (1998). Rho1p–Bni1p–Spa2p interactions: implication in localization of Bni1p at the bud site and regulation of the actin cytoskeleton in Saccharomyces cerevisiae. Mol. Biol. Cell *9*, 1221–1233.

Gietz, R.D., and Sugino, A. (1988). New yeast-*Escherichia coli* shuttle vectors constructed with in vitro mutagenized yeast genes lacking six-base pair restriction sites. Gene *74*, 527–534.

Gladfelter, A.S., Pringle, J.R., and Lew, D.J. (2001). The septin cortex at the yeast mother-bud neck. Curr. Opin. Microbiol. *4*, 681–689.

Goud, B., Salminen, A., Walworth, N.C., and Novick, P.J. (1988). A GTP-binding protein required for secretion rapidly associates with secretory vesicles and the plasma membrane in yeast. Cell *53*, 753–768.

Guo, W., Grant, A., and Novick, P. (1999). Exo84p is an exocyst protein essential for secretion. J. Biol. Chem. *274*, 23558–23564.

Haarer, B.K., Petzold, A., Lillie, S.H., and Brown, S.S. (1994). Identification of MYO4, a second class V myosin gene in yeast. J. Cell Sci. *107*, 1055–1064.

Hanrahan, J., and Snyder, M. (2003). Cytoskeletal activation of a checkpoint kinase. Mol. Cell *12*, 663–673.

Harris, E.S., Li, F., and Higgs, H.N. (2004). The mouse formin, FRLalpha, slows actin filament barbed end elongation, competes with capping protein, accelerates polymerization from monomers, and severs filaments. J. Biol. Chem. *297*, 20076–20087.

Hartwell, L.H. (1971). Genetic control of the cell division cycle in yeast. IV. Genes controlling bud emergence and cytokinesis. Exp. Cell Res. *69*, 265–276.

Imamura, H., Tanaka, K., Hihara, T., Umikawa, M., Kamei, T., Takahashi, K., Sasaki, T., and Takai, Y. (1997). Bni1p and Bnr1p: downstream targets of the Rho family small G-proteins which interact with profilin and regulate actin cytoskeleton in Saccharomyces cerevisiae. EMBO J. *16*, 2745–2755.

Jansen, R.P., Dowzer, C., Michaelis, C., Galova, M., and Nasmyth, K. (1996). Mother cell-specific HO expression in budding yeast depends on the unconventional myosin myo4p and other cytoplasmic proteins. Cell *84*, 687–697.

Jaquenoud, M., and Peter, M. (2000). Gic2p may link activated Cdc42p to components involved in actin polarization, including Bni1p and Bud6p (Aip3p). Mol. Cell. Biol. *20*, 6244–6258.

Jin, H., and Amberg, D.C. (2000). The secretory pathway mediates localization of the cell polarity regulator Aip3p/Bud6p. Mol. Biol. Cell *11*, 647–661.

Johnston, G.C., Prendergast, J.A., and Singer, R.A. (1991). The *Saccharomyces cerevisiae* MYO2 gene encodes an essential myosin for vectorial transport of vesicles. J. Cell Biol. *113*, 539–551.

Kamei, T., Tanaka, K., Hihara, T., Umikawa, M., Imamura, H., Kikyo, M., Ozaki, K., and Takai, Y. (1998). Interaction of Bnr1p with a novel Src homology 3 domain-containing Hof1p. Implication in cytokinesis in *Saccharomyces cerevisiae*. J. Biol. Chem. *273*, 28341–28345.

Kikyo, M., Tanaka, K., Kamei, T., Ozaki, K., Fujiwara, T., Inoue, E., Takita, Y., Ohya, Y., and Takai, Y. (1999). An FH domain-containing Bnr1p is a multifunctional protein interacting with a variety of cytoskeletal proteins in *Saccharomyces cerevisiae*. Oncogene *18*, 7046–7054.

Kilmartin, J.V., and Adams, A.E. (1984). Structural rearrangements of tubulin and actin during the cell cycle of the yeast *Saccharomyces*. J. Cell Biol. *98*, 922–933.

Kobielak, A., Pasolli, H.A., and Fuchs, E. (2004). Mammalian formin-1 participates in adherens junctions and polymerization of linear actin cables. Nat. Cell Biol. *6*, 21–30.

Kohno, H., *et al*. (1996). Bni1p implicated in cytoskeletal control is a putative target of Rho1p small GTP binding protein in Saccharomyces cerevisiae. EMBO J. *15*, 6060–6068.

Kovar, D.R., Kuhn, J.R., Tichy, A.L., and Pollard, T.D. (2003). The fission yeast cytokinesis formin Cdc12p is a barbed end actin filament capping protein gated by profilin. J. Cell Biol. *161*, 875–887.

Kozminski, K.G., Chen, A.J., Rodal, A.A., and Drubin, D.G. (2000). Functions and functional domains of the GTPase Cdc42p. Mol. Biol. Cell *11*, 339–354.

Lee, L., Klee, S.K., Evangelista, M., Boone, C., and Pellman, D. (1999). Control of mitotic spindle position by the *Saccharomyces cerevisiae* formin Bni1p. J. Cell Biol. *144*, 947–961.

Lew, D.J., and Reed, S.I. (1993). Morphogenesis in the yeast cell cycle: regulation by Cdc28 and cyclins. J. Cell Biol. *120*, 1305–1320.

Lew, D.J., and Reed, S.I. (1995). Cell cycle control of morphogenesis in budding yeast. Curr. Opin. Genet Dev. *5*, 17–23.

Li, F., and Higgs, H.N. (2003). The mouse Formin mDia1 is a potent actin nucleation factor regulated by autoinhibition. Curr. Biol. *13*, 1335–1340.

Lillie, S.H., and Brown, S.S. (1994). Immunofluorescence localization of the unconventional myosin, Myo2p, and the putative kinesin-related protein, Smy1p, to the same regions of polarized growth in *Saccharomyces cerevisiae*. J. Cell Biol. *125*, 825–842.

Lippincott, J., and Li, R. (1998). Sequential assembly of myosin II, an IQGAP-like protein, and filamentous actin to a ring structure involved in budding yeast cytokinesis. J. Cell Biol. *140*, 355–366.

Liu, H., Krizek, J., and Bretscher, A. (1992). Construction of a GAL1-regulated yeast cDNA expression library and its application to the identification of genes whose overexpression causes lethality in yeast. Genetics *132*, 665–673.

Liu, H.P., and Bretscher, A. (1989). Disruption of the single tropomyosin gene in yeast results in the disappearance of actin cables from the cytoskeleton. Cell *57*, 233–242.

Longtine, M.S., and Bi, E. (2003). Regulation of septin organization and function in yeast. Trends Cell Biol. *13*, 403–409.

Longtine, M.S., DeMarini, D.J., Valencik, M.L., Al-Awar, O.S., Fares, H., De Virgilio, C., and Pringle, J.R. (1996). The septins: roles in cytokinesis and other processes. Curr. Opin. Cell Biol. *8*, 106–119.

Longtine, M.S., McKenzie, A., 3rd, Demarini, D.J., Shah, N.G., Wach, A., Brachat, A., Philippsen, P., and Pringle, J.R. (1998). Additional modules for versatile and economical PCR-based gene deletion and modification in *Saccharomyces cerevisiae*. Yeast *14*, 953–961.

Longtine, M.S., Theesfeld, C.L., McMillan, J.N., Weaver, E., Pringle, J.R., and Lew, D.J. (2000). Septin-dependent assembly of a cell cycle-regulatory module in *Saccharomyces cerevisiae*. Mol. Cell. Biol. *20*, 4049–4061.

MacLean-Fletcher, S., and Pollard, T.D. (1980). Mechanism of action of cytochalasin B on actin. Cell *20*, 329–341.

McCaffrey, M., Johnson, J.S., Goud, B., Myers, A.M., Rossier, J., Popoff, M.R., Madaule, P., and Boquet, P. (1991). The small GTP-binding protein Rho1p is localized on the Golgi apparatus and post-Golgi vesicles in *Saccharomyces cerevisiae*. J. Cell Biol. *115*, 309–319.

McMillan, J.N., Longtine, M.S., Sia, R.A., Theesfeld, C.L., Bardes, E.S., Pringle, J.R., and Lew, D.J. (1999). The morphogenesis checkpoint in *Saccharomyces cerevisiae*: cell cycle control of Swe1p degradation by Hsl1p and Hsl7p. Mol. Cell. Biol. *19*, 6929–6939.

Miller, R.K., Matheos, D., and Rose, M.D. (1999). The cortical localization of the microtubule orientation protein, Kar9p, is dependent upon actin and proteins required for polarization. J. Cell Biol. *144*, 963–975.

Moffat, J., and Andrews, B. (2003). Ac'septin'a signal: kinase regulation by septins. Dev. Cell *5*, 528–530.

Mosch, H.U., and Fink, G.R. (1997). Dissection of filamentous growth by transposon mutagenesis in *Saccharomyces cerevisiae*. Genetics *145*, 671–684.

Moseley, J.B., Sagot, I., Manning, A.L., Xu, Y., Eck, M.J., Pellman, D., and Goode, B.L. (2004). A conserved mechanism for Bni1- and mDia1-induced actin assembly and dual regulation of Bni1 by Bud6 and profilin. Mol. Biol. Cell *15*, 896–907.

Mulholland, J., Wesp, A., Riezman, H., and Botstein, D. (1997). Yeast actin cytoskeleton mutants accumulate a new class of Golgi-derived secretary vesicle. Mol. Biol. Cell *8*, 1481–1499.

Novick, P., Ferro, S., and Schekman, R. (1981). Order of events in the yeast secretory pathway. Cell *25*, 461–469.

Novick, P., Field, C., and Schekman, R. (1980). Identification of 23 complementation groups required for post-translational events in the yeast secretory pathway. Cell *21*, 205–215.

Ozaki-Kuroda, K., Yamamoto, Y., Nohara, H., Kinoshita, M., Fujiwara, T., Irie, K., and Takai, Y. (2001). Dynamic localization and function of Bni1p at the sites of directed growth in *Saccharomyces cerevisiae*. Mol. Cell. Biol. *21*, 827–839.

Petersen, J., Nielsen, O., Egel, R., and Hagan, I.M. (1998). FH3, a domain found in formins, targets the fission yeast formin Fus1 to the projection tip during conjugation. J. Cell Biol. *141*, 1217–1228.

Pring, M., Evangelista, M., Boone, C., Yang, C., and Zigmond, S.H. (2003). Mechanism of formin-induced nucleation of actin filaments. Biochemistry *42*, 486–496.

Pruyne, D., Evangelista, M., Yang, C., Bi, E., Zigmond, S., Bretscher, A., and Boone, C. (2002). Role of formins in actin assembly: nucleation and barbed-end association. Science *297*, 612–615.

Pruyne, D.W., Schott, D.H., and Bretscher, A. (1998). Tropomyosin-containing actin cables direct the Myo2p-dependent polarized delivery of secretory vesicles in budding yeast. J. Cell Biol. *143*, 1931–1945.

Richman, T.J., Sawyer, M.M., and Johnson, D.I. (1999). The Cdc42p GTPase is involved in a G2/M morphogenetic checkpoint regulating the apical-isotropic switch and nuclear division in yeast. J. Biol. Chem. *274*, 16861–16870.

Rua, D., Tobe, B.T., and Kron, S.J. (2001). Cell cycle control of yeast filamentous growth. Curr. Opin. Microbiol. *4*, 720–727.

Russell, D.W., Jensen, R., Zoller, M.J., Burke, J., Errede, B., Smith, M., and Herskowitz, I. (1986). Structure of the *Saccharomyces cerevisiae* HO gene and analysis of its upstream regulatory region. Mol. Cell. Biol. *6*, 4281–4294.

Sagot, I., Klee, S.K., and Pellman, D. (2002a). Yeast formins regulate cell polarity by controlling the assembly of actin cables. Nat. Cell Biol. *4*, 42–50.

Sagot, I., Rodal, A.A., Moseley, J., Goode, B.L., and Pellman, D. (2002b). An actin nucleation mechanism mediated by Bni1 and profilin. Nat. Cell Biol. *4*, 626–631.

Salminen, A., and Novick, P.J. (1987). A ras-like protein is required for a post-Golgi event in yeast secretion. Cell *49*, 527–538.

Schott, D., Ho, J., Pruyne, D., and Bretscher, A. (1999). The COOH-terminal domain of Myo2p, a yeast myosin V, has a direct role in secretory vesicle targeting. J. Cell Biol. *147*, 791–808.

Schott, D.H., Collins, R.N., and Bretscher, A. (2002). Secretory vesicle transport velocity in living cells depends on the myosin-V lever arm length. J. Cell Biol. *156*, 35–39.

Segal, M., Bloom, K., and Reed, S.I. (2000). Bud6 directs sequential microtubule interactions with the bud tip and bud neck during spindle morphogenesis in Saccharomyces cerevisiae. Mol. Biol. Cell *11*, 3689–3702.

Sheu, Y.J., Barral, Y., and Snyder, M. (2000). Polarized growth controls cell shape and bipolar bud site selection in Saccharomyces cerevisiae. Mol. Cell. Biol. *20*, 5235–5247.

Sheu, Y.J., Santos, B., Fortin, N., Costigan, C., and Snyder, M. (1998). Spa2p interacts with cell polarity proteins and signaling components involved in yeast cell morphogenesis. Mol. Cell. Biol. *18*, 4053–4069.

Shulewitz, M.J., Inouye, C.J., and Thorner, J. (1999). Hsl7 localizes to a septin ring and serves as an adapter in a regulatory pathway that relieves tyrosine phosphorylation of Cdc28 protein kinase in *Saccharomyces cerevisiae*. Mol. Cell. Biol. *19*, 7123–7137.

Sikorski, R.S., and Hieter, P. (1989). A system of shuttle vectors and yeast host strains designed for efficient manipulation of DNA in Saccharomyces cerevisiae. Genetics *122*, 19–27.

Snyder, M. (1989). The SPA2 protein of yeast localizes to sites of cell growth. J. Cell Biol. *108*, 1419–1429.

Takizawa, P.A., Sil, A., Swedlow, J.R., Herskowitz, I., and Vale, R.D. (1997). Actin-dependent localization of an RNA encoding a cell-fate determinant in yeast. Nature *389*, 90–93.

TerBush, D.R., Maurice, T., Roth, D., and Novick, P. (1996). The Exocyst is a multiprotein complex required for exocytosis in *Saccharomyces cerevisiae*. EMBO J. *15*, 6483–6494.

TerBush, D.R., and Novick, P. (1995). Sec6, Sec8, and Sec15 are components of a multisubunit complex which localizes to small bud tips in *Saccharomyces cerevisiae*. J. Cell Biol. *130*, 299–312.

Tolliday, N., VerPlank, L., and Li, R. (2002). Rho1 directs formin-mediated actin ring assembly during budding yeast cytokinesis. Curr. Biol. *12*, 1864–1870.

Tong, A.H., *et al*. (2001). Systematic genetic analysis with ordered arrays of yeast deletion mutants. Science *294*, 2364–2368.

Tong, A.H., *et al*. (2004). Global mapping of the yeast genetic interaction network. Science *303*, 808–813.

Vallen, E.A., Caviston, J., and Bi, E. (2000). Roles of Hof1p, Bni1p, Bnr1p, and myo1p in cytokinesis in *Saccharomyces cerevisiae*. Mol. Biol. Cell *11*, 593–611.

Wagner, W., Bielli, P., Wacha, S., and Ragnini-Wilson, A. (2002). Mlc1p promotes septum closure during cytokinesis via the IQ motifs of the vesicle motor Myo2p. EMBO J. *21*, 6397–6408.

Walch-Solimena, C., Collins, R.N., and Novick, P.J. (1997). Sec2p mediates nucleotide exchange on Sec4p and is involved in polarized delivery of post-Golgi vesicles. J. Cell Biol. *137*, 1495–1509.

Wallar, B.J., and Alberts, A.S. (2003). The formins: active scaffolds that remodel the cytoskeleton. Trends Cell Biol. *13*, 435–446.

Wedlich-Soldner, R., Altschuler, S., Wu, L., and Li, R. (2003). Spontaneous cell polarization through actomyosin-based delivery of the Cdc42 GTPase. Science *299*, 1231–1235.

Winter, D.C., Choe, E.Y., and Li, R. (1999). Genetic dissection of the budding yeast Arp2/3 complex: a comparison of the in vivo and structural roles of individual subunits. Proc. Natl. Acad. Sci. USA *96*, 7288–7293.

Yamochi, W., Tanaka, K., Nonaka, H., Maeda, A., Musha, T., and Takai, Y. (1994). Growth site localization of Rho1 small GTP-binding protein and its involvement in bud formation in *Saccharomyces cerevisiae*. J. Cell Biol. *125*, 1077–1093.

Yang, H.C., and Pon, L.A. (2002). Actin cable dynamics in budding yeast. Proc. Natl. Acad. Sci. USA *99*, 751–756.

Zahner, J.E., Harkins, H.A., and Pringle, J.R. (1996). Genetic analysis of the bipolar pattern of bud site selection in the yeast *Saccharomyces cerevisiae*. Mol. Cell. Biol. *16*, 1857–1870.

Ziman, M., Preuss, D., Mulholland, J., O'Brien, J.M., Botstein, D., and Johnson, D.I. (1993). Subcellular localization of Cdc42p, a *Saccharomyces cerevisiae* GTP-binding protein involved in the control of cell polarity. Mol. Biol. Cell *4*, 1307–1316.